CHAPTER ONE

Photocatalytic Water Splitting on Semiconductor-Based Photocatalysts

Rengui Li, Can Li[1]

State Key Laboratory of Catalysis, Dalian Institute of Chemical Physics, Chinese Academy of Sciences, Dalian National Laboratory for Clean Energy, Collaborative Innovation Center of Chemistry for Energy Materials (iChEM), Dalian, Liaoning, China

[1]Corresponding author: e-mail address: canli@dicp.ac.cn

Contents

Abstract

Photocatalytic hydrogen production via solar water splitting is one of the most promising solutions for sustainable energy and environmental remedy issues. In the past few

Advances in Catalysis, Volume 60
ISSN 0360-0564
https://doi.org/10.1016/bs.acat.2017.09.001

decades, photocatalytic water splitting has attracted increasing attention, and extensive efforts have been made to construct efficient heterogeneous water-splitting systems. In this chapter, we review the fundamental scientific advances in photocatalytic water splitting using semiconductor-based photocatalyst, especially in light-absorbing materials, photogenerated charge separation, dual-cocatalyst, and surface catalytic reactions. The chapter focuses on the advances achieved in particulate photocatalyst systems, Z-scheme photocatalyst systems, and hybrid natural–artificial photosynthesis systems. Additionally, technical and economic evaluation of hydrogen production via solar water splitting for potential applications is also briefly discussed. Finally, we present concluding remarks and future directions of photocatalytic water splitting for solar energy conversion.

1. INTRODUCTION

Energy harvested from sunlight offers a promising approach toward fulfilling the need for clean energy with minimal environmental impact. Solar energy is a decentralized but inexhaustible natural energy resource, with the magnitude of the available solar power striking the earth's surface at any one instant equal to a 130 million 500 MW power plant *(1)*. Capturing and storing solar energy in forms of chemicals (e.g., H_2), as natural photosynthesis in green plants does, are highly desirable approaches for the storage and utilization of solar energy in sustainable development of the world. Hydrogen energy is the cleanest energy with many potential applications, including powering of vehicles, fuel cell, domestic heating, and aircraft, etc. *(2–4)* Additionally, the utilization of hydrogen as an energy carrier is a long-term option to reduce the worldwide CO_2 emissions by CO_2 hydrogenation to value-added chemicals *(5–7)*. Therefore, photocatalytic hydrogen production via solar water splitting is one of the most promising solutions for sustainable energy and environmental issues.

Since the work reported by Fujishima and Honda in 1972 using rutile titanium dioxide (TiO_2) anode coupled with a platinum cathode for photoassisted electrolytic water splitting *(8)*, extensive efforts have been made to construct efficient heterogeneous water splitting systems. For particulate photocatalytic water-splitting system, the photocatalyst powders are dispersed in water under light irradiation, which is an equipment-simple and low-cost way for potential scalable solar hydrogen production. Natural photosynthesis provides the blueprint for the conversion and storage of solar energy in the form of chemical fuels (e.g., glucose, cellulose). In nature photosynthesis system, the light reaction to split water is the primary step, where the photogenerated holes are captured by the oxygen-evolving complex

(Mn_4CaO_5) to oxidize water to dioxygen and protons, which directly pushes the energy-storing chemical process for further synthesis of chemicals. Hence, photocatalytic water splitting is also regarded as a kind of artificial photosynthesis in a broad view of solar energy to chemical energy conversion and recognized as an attractive and challenging topic, a "holy grail" in the field of chemistry.

2. PRINCIPLES OF PHOTOCATALYTIC WATER SPLITTING

Thermodynamically, the overall water-splitting reaction is an energetically uphill and endothermic reaction with a standard Gibbs free energy change (ΔG_0) of 237 kJ/mol (shown in Eq. 1).

$$H_2O \rightarrow H_2 + {}^1/_2O_2,\ \Delta G = 237\,\text{kJ/mol}. \quad (1)$$

Generally, a photocatalytic water-splitting reaction involves three major steps: (i) photocatalysts are photoexcited to generate electrons and holes, (ii) the photogenerated electrons and holes are separated and transferred to the surface of the photocatalysts, and (iii) the photogenerated electrons and holes are captured by the reaction sites on reduction and oxidation cocatalysts and consumed by catalytic reactions for water reduction and oxidation, respectively (Fig. 1) *(9–11)*. The overall efficiency of solar energy

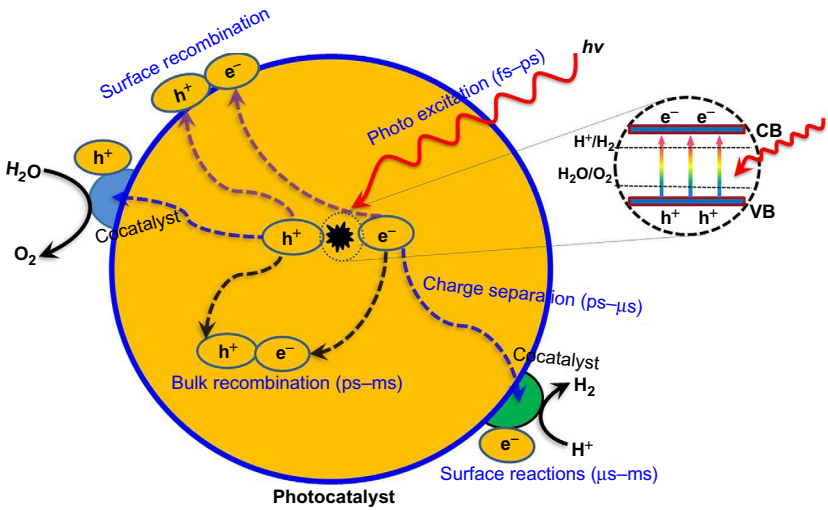

Fig. 1 The mechanism of photocatalytic water splitting on semiconductor-based photocatalyst *(9)*.

conversion is directly determined by the multiplication of the efficiencies of light-harvesting, charge separation, and charge utilization processes (Eq. 2)

$$\eta = \eta_1 \cdot (\eta_2 \times \eta_3) \tag{2}$$

(η_1, efficiency of light harvesting; η_2, efficiency of charge separation; η_3, efficiency of surface catalytic reaction).

The whole water-splitting process on semiconductor-based photocatalysts generally spans more than 10 orders of magnitude timescale from initial light absorption to the end of the surface catalytic reactions to produce H_2 and O_2. Due to the loss of majority of the charges through recombination, the water-splitting efficiencies reported so far are usually relatively low.

Semiconductors possess specific band structures with a band gap usually in the energy range 0.2–4.0 eV. When the photon energy of incident light is equivalent to or larger than the band gap, the electrons in the valence band (VB) are excited to the conduction band (CB), while the holes are left in the valence band. The photoexcited electrons and holes are subsequently relaxed and transport to the surface for the reduction and oxidation reactions, respectively. Water molecules are oxidized by the holes to protons and O_2, and the released protons are reduced by the electrons to H_2. The surface reduction and oxidation reactions for H_2 and O_2 production are similar to water electrolysis reactions. Generally, the bottom level of the conduction band (or lowest unoccupied molecular orbital of an organic complex photocatalyst) has to be more negative than the redox potential of H^+/H_2 (0 V vs RHE), while the top level of the valence band (or highest occupied molecular orbital of an organic complex photocatalyst) should be more positive than the chemical redox potential of O_2/H_2O. That is to say, the minimum Gibbs free energy requirement for water splitting is 1.23 eV, corresponding to a photo in ~1000 nm optical range. Taking consideration of overpotential for the surface redox reactions of water splitting, especially for water oxidation, the band gap of photocatalyst is required to be larger than 1.23 eV in practice.

To efficiently convert solar energy by semiconductor-based photocatalyst, first, the photocatalyst should possess suitable band gap to satisfy not only efficient light absorption but also suitable CB and VB levels for water-splitting redox reactions. Second, an ideal photocatalyst should be highly efficient for the separation and transfer of photogenerated charges. The charge separation and recombination are competitive processes in photocatalysis. Generally, the recombination of photoexcited charges occurs at a very fast timescale (ps–μs). Therefore, the water-splitting redox reactions on

the surface must proceed within the lifetimes of photoexcited charges *(12)*. Efficient separation and transfer of photogenerated charges are critically important for photocatalytic water splitting. Any approaches beneficial to the charge separation should be useful for designing and constructing highly efficient photocatalyst systems. Third, the electrons and holes should be quickly captured by the surface active sites and participate in the reactions with adsorbed species. Surface reaction generally takes places at the longer timescale (μs–s) compared with charge generation and separation processes. So strategies for boosting the surface catalytic reactions are also essential for the construction of an efficient photocatalyst system. Loading proper cocatalysts on the surface of a semiconductor photocatalyst to provide active sites is an effective strategy for accelerating the catalytic reaction and consequently resulting in the improvement of the efficiency of overall water splitting. It should be emphasized that the processes of charge separation and surface catalytic reactions are not independent but synergistically correlated to each other. The faster surface reaction is beneficial for more efficient charge separation and vice versa.

3. QUANTUM EFFICIENCY AND SOLAR-TO-HYDROGEN EFFICIENCY

Quantum yield, defined as the rate at which molecules undergo a given event per photons absorbed per unit time, is well known in photochemistry. Photochemists routinely determine quantum yields of reactant disappearance, product formation, light emission, and various other photochemical and photophysical events occurring in photochemical reactions *(13)*. In heterogeneous photocatalysis, quantum efficiency has come to define the number of reacted electrons relative to the total number of photons incident in the reaction system, for undefined reactor geometry and for polychromatic radiation, rather than the number of absorbed photons at a given wavelength to satisfy the photochemical definition in homogeneous photochemistry. Quantum efficiency in heterogeneous media can be estimated in the same manner as for homogeneous photochemistry if the number of actual absorbed photons or the fraction of light absorbed by the solid photocatalyst can be assessed.

Because the photoactivity for a photocatalyst strongly depends on the experimental conditions (light intensity, reaction temperature, etc.), the activities are usually difficult to be compared with each other *(14)*. It should be noted that the actual quantum efficiency should be internal quantum efficiency (IQE), which is calculated from reacted electrons divided by the

absorbed photons. However, it is hard to determine the amount of photons absorbed by a particulate photocatalyst in a dispersed system because of light scattering and loosing. Generally, a thermopile or Si photodiode can be used to determine the incident photons under the same conditions with H_2 or O_2 gas generated on specific photocatalyst system. So, the obtained quantum efficiency is an apparent quantum efficiency (AQE) at specific monochromatic wavelength *(15)*. The AQE of photocatalyst can be calculated as follows.

$$\begin{aligned} \mathrm{AQE} &= \frac{\text{number of reacted electrons}}{\text{number of incidents photons}} \times 100\% \\ &= \frac{2 \times \text{number of evoluted } H_2 \text{ molecules}}{\text{number of incident photons}} \times 100\% \\ &= \frac{4 \times \text{number of evoluted } O_2 \text{ molecules}}{\text{number of incident photons}} \times 100\% \end{aligned} \tag{3}$$

$$\begin{aligned} \mathrm{IQE} &= \frac{\text{number of reacted electrons}}{\text{number of absorbed photons}} \times 100\% \\ &= \frac{2 \times \text{number of evoluted } H_2 \text{ molecules}}{\text{number of absorbed photons}} \times 100\% \\ &= \frac{4 \times \text{number of evoluted } O_2 \text{ molecules}}{\text{number of absorbed photons}} \times 100\% \end{aligned} \tag{4}$$

Solar-to-hydrogen (STH) efficiency can be used as a practical standard to measure the performance of photocatalysts. The STH efficiency can be calculated as follows:

$$\mathrm{STH} = \frac{\text{output energy as } H_2 \text{ gas}}{\text{energy of incident solar light}} = \frac{r_{H_2} \times \Delta G}{P_{\mathrm{sun}} \times S} \times 100\% \tag{5}$$

where r_{H_2} is the rate of hydrogen production (mmol/s), P_{sun} is energy flux of the sunlight (mW/cm^2), S is the area of the reactor (cm^2), and ΔG is the gain in Gibbs free energy (J/mol).

4. OVERALL WATER SPLITTING AND (H_2 OR O_2 EVOLUTION) HALF REACTIONS

The photocatalytic water-splitting performance can be evaluated by examining the efficiencies of overall water splitting without any sacrificial reagents. In overall water splitting, H_2 and O_2 are produced simultaneously in 2:1 stoichiometric ratio (Eqs. 6–7). To investigate the kinetics of proton reduction or water oxidation half reaction, sacrificial reagents are introduced

to quickly consume the photogenerated holes or electrons in order to make the corresponding half reaction not the rate determining step (Fig. 2). For example, methanol, lactic acid, or triethanol amine, etc. is usually used as hole scavenger for H_2 production half reaction (Eqs. 8–9) and Ag^+, Fe^{3+}, or IO_3^-, etc. are used as electron scavenger for O_2 evolution half reaction (Eqs. 10–11). Two factors to be considered for the half reactions are: (1) to qualitatively estimate if the conduction band or valence band of a specific photocatalyst is thermodynamically sufficient enough for proton reduction or water oxidation; (2) to determine the kinetic reaction rates of proton reduction and water oxidation at actual conditions.

Overall water splitting:

$$4H^+ + 4e^- \rightarrow 2H_2 (\text{reduction reaction}) \quad (6)$$

$$2H_2O + 4h^+ \rightarrow 4H^+ + O_2 (\text{oxidation reaction}) \quad (7)$$

H_2 production half reaction in the presence of sacrificial reagent, taking CH_3OH as an example:

$$6H^+ + 6e^- \rightarrow 3H_2 (\text{reduction reaction}) \quad (8)$$

$$H_2O + CH_3OH + 6h^+ \rightarrow CO_2 + 6H^+ (\text{oxidation reaction}) \quad (9)$$

O_2 evolution half reaction in the presence of sacrificial reagent, taking Ag^+ as an example:

$$4Ag^+ + 4e^- \rightarrow 4Ag (\text{reduction reaction}) \quad (10)$$

$$2H_2O + 4h^+ \rightarrow 4H^+ + O_2 (\text{oxidation reaction}) \quad (11)$$

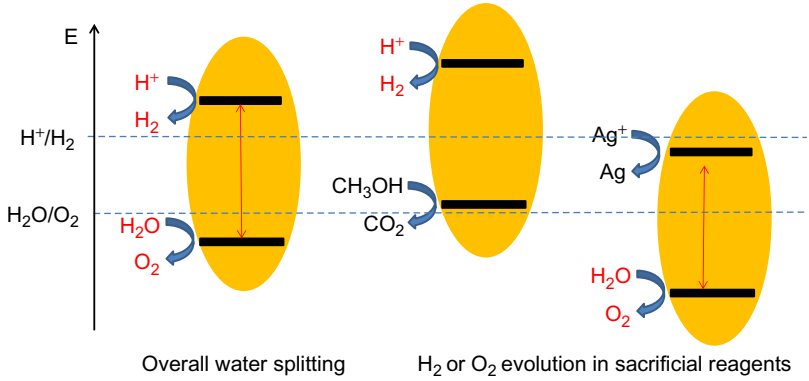

Fig. 2 Scheme of photocatalytic overall water splitting and half reactions in the presence of sacrificial reagents.

5. LIGHT-HARVESTING OF PHOTOCATALYSTS

Many semiconductor-based photocatalysts have shown to be active for photocatalytic water splitting under UV or visible light irradiation. On the basis of the electronic configuration, these photocatalysts can be classified into two main groups: one is the metal oxides with the electronic structure of metal in d^0 configuration (Ti^{4+}, Zr^{4+}, Nb^{5+}, Ta^{5+}, W^{6+}, Mo^{6+}, etc.), and the other is the metal oxides with the electronic structure of metal in d^{10} configuration (In^{3+}, Ga^{3+}, Ge^{4+}, Sn^{4+}, Sb^{5+}, etc.) *(14)*.

5.1 UV Light-Responsive Photocatalysts

Most of the UV light-responsive photocatalysts capable of water splitting are metal oxides contain metals with d^0 and d^{10} configurations. For these semiconductors, the conduction band minimum is usually composed of d and sp orbitals of metals, while the valence band maximum is contributed by O 2p orbitals.

Titanium-based photocatalysts is one kind of the widely investigated materials for water splitting. TiO_2 is a representative photocatalyst in this field. Although photoelectrochemical water splitting has been achieved on TiO_2 photoanode with bias voltage, particulate TiO_2 photocatalyst cannot split water without the assistance of cocatalysts. For a platinized TiO_2 photocatalyst, evolution of only H_2 but no O_2 was often observed in the absence of any sacrificial reagents. It has also been reported that NaOH-coating or addition of alkali carbonates was effective for water splitting on Pt/TiO_2 photocatalyst *(15)*. Only recently, direct splitting of pure water into hydrogen and oxygen using rutile TiO_2 powder was reported *(16,17)*, indicating that the overall water splitting on TiO_2 photocatalyst is closely related to its crystalline phase structure. Shortly after this work, the overall water splitting on anatase and brookite TiO_2 was also reported to be possible if TiO_2 samples are treated with prolonged UV light irradiation *(17)*. Strontium titanate ($SrTiO_3$) with light absorption edge at ca. 400 nm (band gap of 3.2 eV) is another typical and important titanium-based photocatalyst for overall water splitting. The effects of morphology, doping, and crystalline facet of $SrTiO_3$ on photocatalytic water splitting have been investigated in detail *(18–20)*. The highest AQE for $SrTiO_3$ was reported to be 30% at 360 nm by doping Al in the bulk using flux treatment *(21)*. $ALa_xTi_yO_z$ (A = K, Ba, Sr, Ca), a series of photocatalysts with layered perovskite structure, has also been reported for both photocatalytic water splitting

and CO_2 reduction, and its photocatalytic activity is found to be strongly dependent on the type of the alkaline earth metal ions *(22)*.

Tantalum-based photocatalysts are also effective for water splitting. Kato et al. reported that alkali tantalate $ATaO_3$ (A = Li, Na, and K) photocatalysts with perovskite-like structure are active for water splitting under UV irradiation *(23)*. It was found that photocatalytic activities, as well as the band gaps, are largely dependent on the A site cation of the perovskite-like structure. After loading NiO on $NaTaO_3$ doped with lanthanum, the maximum AQE reached 56% at 270 nm *(24)*. Ta_2O_5 photocatalysts loaded with RuO_2 or NiO cocatalyst were also found to be able to decompose water into H_2 and O_2 *(25)*. $K_3Ta_3Si_2O_{13}$ or $K_3Ta_3Bi_2O_{12}$ with pillared structure, in which three linear chains of corner shared TaO_6 are connected with each other, is an active photocatalyst for water splitting. And the photocatalytic activity for water splitting can be drastically increased by loading a small amount of NiO cocatalyst *(26,27)*. Orthorhombic ATa_2O_6 (A = Ca, Sr, Ba) prepared by flux treatment was also reported to be UV-responsive photocatalyst, and $SrTa_2O_6$ shows an AQE of ~7% for overall water spitting *(28)*.

Niobium-containing semiconductors have been proven to be effective photocatalysts due to their special distortable (NbO_6) octahedral structure, and the fairly high energy level of Nb 4d which is beneficial for providing high driving force for hydrogen production *(14)*. $K_4Nb_6O_{17}$ is an ion-exchangeable layered compound with a band gap of 3.3 eV *(29)*. Upon loading NiO cocatalyst, photocatalytic water-splitting activity was achieved. $Sr_2Nb_2O_7$ is a layered perovskite structure with band gap of 4.0 eV, which shows photocatalytic water-splitting activities without any additives under UV irradiation *(30)*. It was suggested that the dipole moment along the perovskite layers seems to play an important role in photogenerated charge separation and consequently contributes to its overall water splitting. Some other Nb-based photocatalysts, such as $ZnNb_2O_6$ *(31)*, $Ba_5Nb_4O_{15}$ *(32)*, and La_3NbO_7 *(33)*, were also reported to be capable for photocatalytic overall water splitting under UV light irradiation.

ZrO_2 powder was reported to be able to photocatalytic decomposition of pure water, and the rates of H_2 and O_2 evolution can be further increased upon addition of Na_2CO_3 and $NaHCO_3$ *(34)*. This photocatalyst is also active for CO_2 reduction to CO with water as the electron source, as evidenced by the O_2 evolution via water oxidation. Highly negative flat-band potential and wide band gap were regarded to be the main beneficial character of ZrO_2 as photocatalyst.

Some p-block metal oxides are found to be useful photocatalysts for overall water splitting, for example, MIn_2O_4 (M = Ca, Sr), Sr_2SnO_4, and $NaSbO_3$ with RuO_2 loaded as cocatalyst *(35)*. The valence bands of these photocatalysts are composed essentially of the oxygen 2p orbitals. The d orbital levels are so deep that the inner d electrons have little influence on the excitation from the O 2p bands to the conduction levels which are usually composed of the p-block orbitals.

5.2 Visible Light-Responsive Photocatalysts

As less than 5% of solar light is in UV region, the light absorption by photocatalysts should be extended to longer wavelength in order to harness more sunlight, especially visible light which is the most intense and occupies more than 40% of solar light energy. In view of this point, band engineering to narrow the band gap of semiconductor photocatalysts is important to the light harvesting. In order to narrow the band gap of metal oxide photocatalysts, band engineering by introducting foreign elements is an effective approach as shown in Fig. 3.

For valance band engineering, a new valence band or an electron donor level must be formed with orbitals of elements other than O 2p. In order to split water, not only the thermodynamic potential but also the kinetics of four-electron transfer for the oxidation of water is required. The typical and widely used examples include oxynitride or oxysulfide photocatalysts, and their valence band is usually composed of N 2p or S 3p hybrid with O 2p orbitals (Fig. 4). These different anions introduced usually replace the O sites. For example, introduction of N to replace a part of O atoms in TiO_2 results the visible light-responsive ($\lambda < 500$ nm) photocatalytic activity as reported by Asahi et al. *(36)*. Liu et al. codoped B and N elements into TiO_2 and enhanced the visible light absorption of TiO_2 *(37)*. $MgTa_2O_6$ is a typical

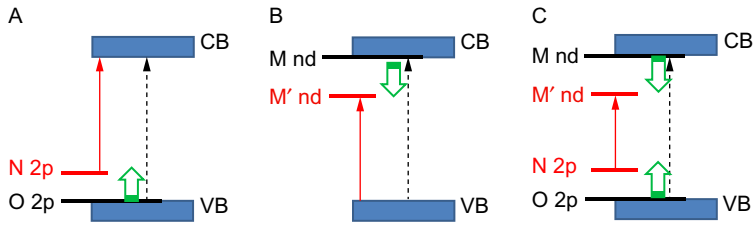

Fig. 3 Strategies for band engineering of semiconductors: (A) modification of valance band, (B) modification of conduction band, and (C) changing both valance band and conduction band by formation of solid solution.

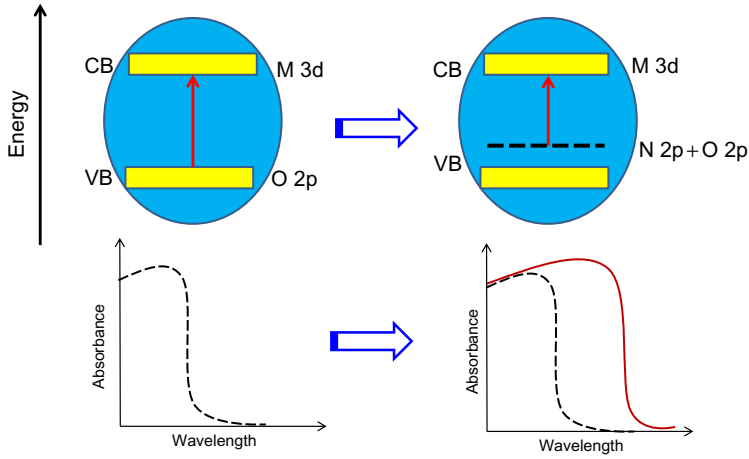

Fig. 4 Schematic description of introducing N orbital in valence band to narrow the band gap of photocatalysts.

dielectric oxide with the capability of water splitting under UV light irradiation. The TaO_6 octahedrons share corners and edges to form a three-dimensional framework possessing tunnels running down the *b*-axis in which the Mg cations are located. Such tunnel structure is beneficial for gas diffusion, so in preparation upon nitridation by NH_3 treatment, the nitrogen-doping can be relatively easy and the light absorption of the nitrogen doped samples $MgTa_2O_{6-x}N_x$ shows an absorption edge at ca. 570 nm, which is greatly shifted from the pristine $MgTa_2O_6$ at only 300 nm to over 500 nm *(38)*. Such $MgTa_2O_{6-x}N_x$ photocatalyst was demonstrated to be effective for both water oxidation and reduction half reactions under visible light irradiation. Similar results were also reported for layered oxide $Sr_5Ta_4O_{15-x}N_x$ *(39)*. Visible light-responsive photocatalyst TaON ($\lambda \leq 500$ nm) can be prepared by nitridation of Ta_2O_5 in NH_3 gas atmosphere at high temperature *(40)*. The bottom of the conduction band of TaON is composed of Ta 5d orbitals similar to Ta_2O_5, whereas the top of the valence band is contributed by hybridization of N 2p and O 2p orbitals. The potential of the hybridized orbital is higher than that of an O 2p orbital in an oxide, resulting in smaller band gap sufficient to absorb visible light. Further nitridation treatment of TaON to completely replace the remaining O by N will form Ta_3N_5, which can absorb visible light to the edge of ~650 nm *(41)*. By using such a doping strategy, a series of metal oxynitrides and metal nitrides with suitable band structures for overall water splitting under visible light irradiation have been prepared. Fig. 5 gives some potential visible light-responsive (from ~480 to ~700 nm) oxynitride

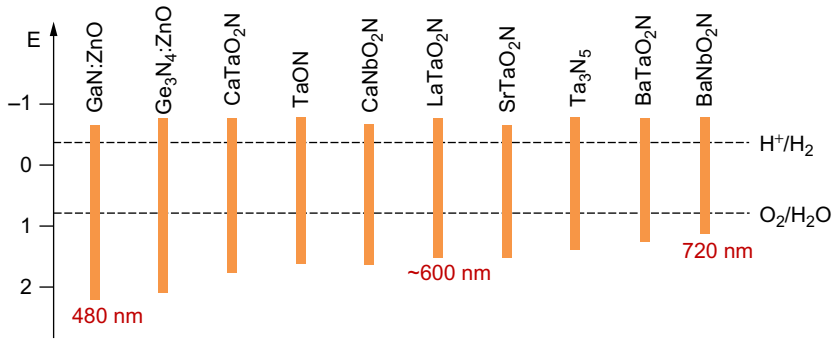

Fig. 5 Some examples of oxynitride photocatalysts as potential candidates for water splitting.

photocatalysts (e.g., TaON, $LaTaO_2N$, $BaNbO_2N$) for photocatalytic water splitting.

In addition to the introduction of N 2p orbital in oxides, hybridization of S 3p orbital with O 2p orbital of valance bands is also demonstrated to be useful to narrow the band gap of oxide-based photocatalysts. Ishikawa et al. prepared a Ti-based oxysulfide $Sm_2Ti_2S_2O_5$ by sulfidation of the Ti-based oxide photocatalyst under H_2S flow *(42)*. The $Sm_2Ti_2S_2O_5$ photocatalyst possesses a band gap of ~2 eV and suitable band positions for both H_2 and O_2 evolution under visible light irradiation. The S 3p orbitals constitute the top of the valence band which is the contribution to the small band gap energy of $Sm_2Ti_2S_2O_5$. Following this work, a series oxysulfide photocatalysts $Ln_2Ti_2S_2O_5$ (Ln = Pr, Nd, Gd, Tb, Dy, Ho, and Er) with similar light-absorption properties and band gaps of $Sm_2Ti_2S_2O_5$ were reported *(43)*. Another type of titanium-based oxysulfide photocatalysts, $La_5Ti_2MS_5O_7$ (M = Ag, Cu), which can absorb visible light up to 570 nm (M = Ag) and 650 nm (M = Cu), were found to be efficient photocatalysts for both water reduction and oxidation *(44)*.

For the strategy of conduction band engineering, the substitution of alkali metal or alkaline-earth metal is useful in lowering the minimum of the conduction band. Taking $AgMO_2$ (M = Al, Ga, In) photocatalyst as an example, Ouyang and coworkers found that it is reasonable for band gap narrowing in this system varied in the order of Al, Ga, and In *(45)*. The conduction bands of $AgMO_2$ are mainly constituted of Ag 5s5p and M sp orbitals, and the valence bands are composed of the Ag 4d and O 2p orbitals. The conduction bands vary with changing the composite M from Al to In, leading to the results that the band gaps of α-$AgMO_2$ (M = Al, Ga, In) were controlled from 2.38 to 1.90 eV. Similarly, the ratio

varying of Al and Ga elements in β-$Ag_{1-x}Ga_xO_2$ allows the bottom of the conduction band to be continuously tuned in the range of 2.19 and 2.83 eV (Fig. 6) *(46)*.

Both conduction and valance bands could be tuned by formating solid solutions. For example, although GaN and ZnO can only absorb UV light (less than 380 nm), GaN:ZnO solid solution is active for both proton reduction and water oxidation under visible light irradiation, which is a representative photocatalyst that can achieve overall water splitting under visible light (Fig. 7) *(47)*. The GaN:ZnO is generally prepared by NH_3 treatment of a mixture of Ga_2O_3 and ZnO at high temperature (generally higher than 1000 K). The visible light absorption is due to a Zn-related acceptor level and/or p–d repulsion between Zn 3d and N 2p + O 2p in addition to the contribution of N 2p to valence band formation *(48)*. Similar strategy was also found to be useful for Ge_3N_4:ZnO solid solution which exhibits a band gap of ca. 2.7 eV *(49)*.

It should be noted that doping some metallic or nonmetallic elements in the crystalline structure of semiconductor photocatalysts is possible to tune the electronic structures and consequently leads to the change of light absorption properties. However, the doping strategy may also have a

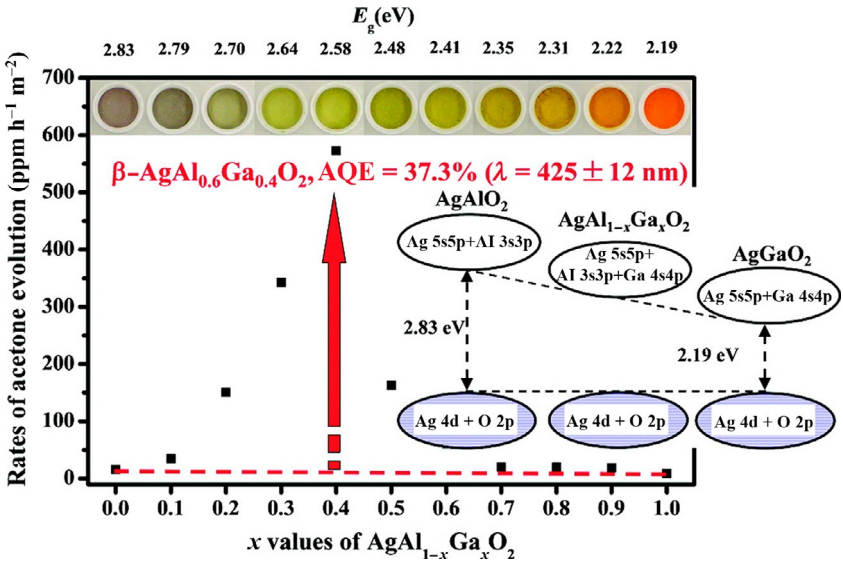

Fig. 6 Tuning conduction band of $AgAlO_2$ for narrowing the band gap of photocatalyst. *Reprinted (adapted) with permission from Ouyang, S. X.; Ye, J. H.* J. Am. Chem. Soc. ***2011***, 133, *7757–7763. Copyright (2011) American Chemical Society.*

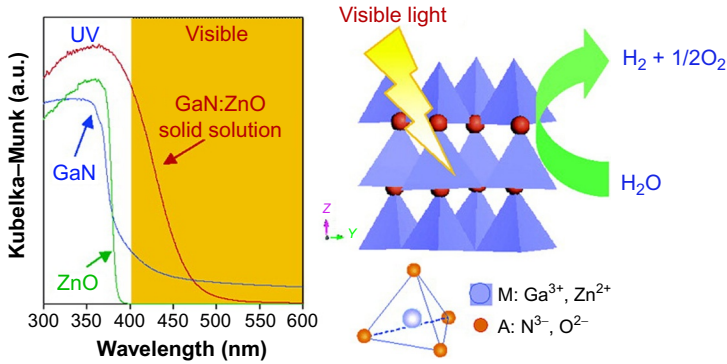

Fig. 7 Light absorption properties of bare GaN, ZnO, and GaN:ZnO solid solution photocatalysts. *Reprinted (adapted) with permission from Maeda, K.; Takata, T.; Hara, M.; Saito, N.; Inoue, Y.; Kobayashi, H.; Domen, K.* J. Am. Chem. Soc. ***2005***, 127, *8286–8287. Copyright (2005) American Chemical Society.*

negative effect in photocatalysis. In many cases, although the doping of some elements changes the light absorption range of photocatalyst, the photocatalytic activity drastically decreases because of formation of recombination centers for photogenerated electrons and holes.

6. PHOTOGENERATED CHARGE SEPARATION

Absorption of photons by photocatalyst induces the generation of photoexcited electrons and holes. The photogenerated electrons and holes should be then separated and transferred to surface for reduction and oxidation reactions, respectively. Therefore, separation of photogenerated charge carriers is one of the most critical factors affecting the efficiency of fuels production. Improving the charge separation efficiency by reducing the charge recombination is a challenging and long-standing issue in photocatalysis. Bulk/surface defects of photocatalyst usually act as the recombination centers for photoexcited electrons and holes, therefore, increasing the crystallinity of photocatalysts can reduce the probability of charge recombination by diminishing these recombination centers. Reducing the particle size of a photocatalyst may also decrease the recombination probability because it shortens the diffusion pathway of the charge carriers *(50)*. Various strategies for charge separation have been explored for reducing bulk or surface recombination in both single particle and composite photocatalyst systems.

6.1 Strategies for Enhancing the Efficiency of Charge Separation

Various strategies have been applied to increase the charge separation efficiency of semiconductor-based photocatalysts. Construction of junctions (heterojunction, phase junction, and Schottky junction) has been well recognized as an effective strategy for the separation of photogenerated charge carriers in semiconductors. In the meantime, strategy for charge separation in a single semiconductor-based photocatalyst will be also discussed in this section.

6.1.1 p–n Junction and Heterojunction

It has been well demonstrated in silicon-based solar cell that p–n junction is an effective strategy for photogenerated charge separation. In a p–n junction-based photocatalyst, p–n junction is formed at the interface of two semiconductors, in which space-charge region originated from the diffusion of electrons and holes forms a built-in electric filed. The built-in electric field can provide the driving force for the separation of photogenerated electrons and holes to migrate to the opposite direction. As shown in Fig. 8, the electrons prefer to transfer to the conduction band of the n-type semiconductors and the holes to the valance band of the p-type semiconductors *(51,52)*. The junction results in a more effective charge separation, which leads to a longer lifetime of the charge carriers for participating in reduction and oxidation reactions. As early as in 1970s, Nozik constructed an n-TiO_2/p-GaP photoelectrode for photoelectrolysis of water and such photoelectrode was found to be much more active than either n-TiO_2 or p-GaP single-component electrode for the splitting of water to H_2 and O_2 without the need of external bias *(53)*. Following this principle, more and more composite photocatalysts containing p–n junction for charge separation have been investigated. For example, Chen et al.

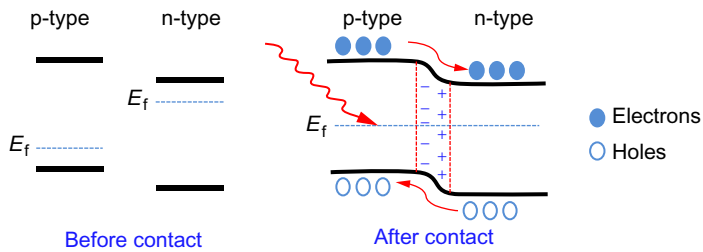

Fig. 8 Scheme of photogenerated charge separation induced by p–n junction formed between p-type and n-type semiconductors.

reported a photocatalyst constructed by p-type ZnO and n-type TiO_2 (ZnO/TiO_2) which shows a remarkable enhancement in photocatalytic reduction of $Cr_2O_7^{2-}$ ions *(54)*. Kim et al. fabricated a composite photocatalyst containing nanoislands of p-type $CaFe_2O_4$ over a highly crystalline layered perovskite photocatalyst, n-type $PbBi_2Nb_{1.9}W_{0.1}O_9$, forming a p–n junction interface between two semiconductors, which shows great enhancement in both photocatalytic activity and stability under visible light irradiation *(55)*. Kim and Lee et al. fabricated p–n junction between p-type $CaFe_2O_4$ and n-type $MgFe_2O_4$ photocatalyst, which has demonstrated to be highly active for photocatalytic hydrogen production from water under visible light irradiation *(56)*.

The junction strategy for photogenerated charge separation has been widely extended to composite photocatalysts constructed by two semiconductors with different band structures or Femi levels denoted as heterojunction. Heterojunction photocatalysts, including TiO_2/CdS *(57,58)*, $BiVO_4/WO_3$ *(59–61)*, TiO_2/CdTe *(62,63)*, α-Fe_2O_3/TiO_2 *(64,65)*, $SrTiO_3/Cu_2O$ *(66)*, $SrTiO_3/\alpha$-Fe_2O_3 *(67)*, and α-Fe_2O_3/WO_3 *(68)*, have shown enhanced activities of photocatalytic or photoelectrochemical water splitting. Su and Grimes et al. fabricated a nanostructured $BiVO_4/WO_3$ heterojunction photoanode, which shows superior photocurrent and stability for photoelectrochemical water splitting than bare $BiVO_4$ or WO_3 photoeletrode *(60)*. It was found that faster charge separation induced by the nanostructured heterojunction reduces charge recombination and hence improves the overall phototocurrent conversion efficiency. Sivula et al. reported that higher activity of photoelectrochemical water oxidation on α-Fe_2O_3/WO_3 photoelectrode due to existence of intact hematite/electrolyte interface allowing more photogenerated holes to transfer to the semiconductor–liquid junction for surface reactions *(69)*.

6.1.2 Phase Junction

Polymorph semiconductors possess different crystalline phases with slightly different physicochemical properties. For example, TiO_2 has three common crystalline structures, anatase, rutile, and brookite. An interesting phenomenon of TiO_2 is that the highest photocatalytic activity is usually not obtained for its pure crystalline forms, either anatase or rutile, but from samples with a mixture of anatase and rutile phases. P25, a commercial TiO_2 material with mixed anatase and rutile phases, is a typical benchmark photocatalyst in environmental purification, self-cleaning, and other photocatalytic reactions. To understand the role of crystalline phases in

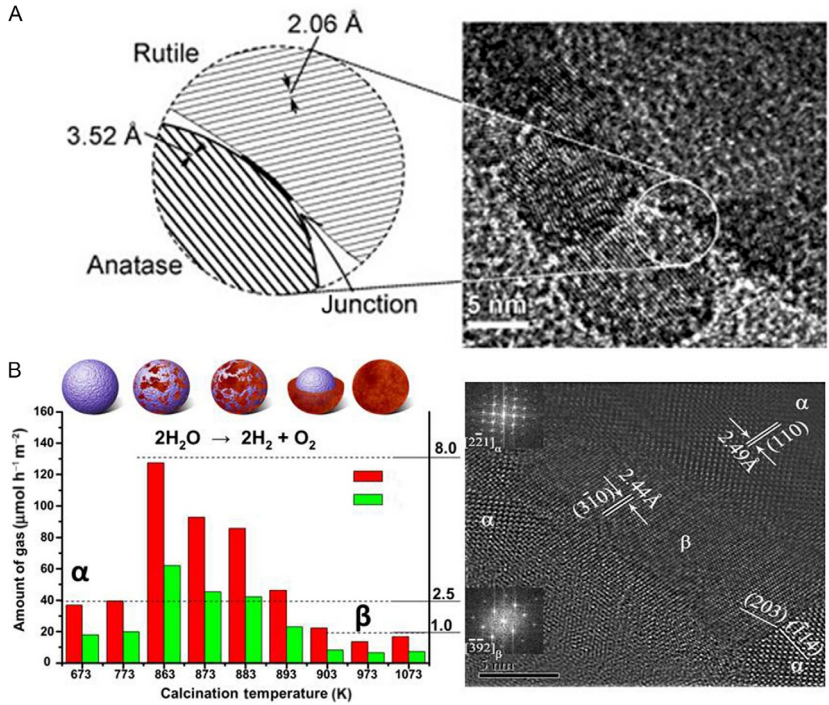

Fig. 9 Examples of phase junction strategies for promoting photogenerated charge separation in photocatalytic water splitting. (A) Phase junction between anatase and rutile phase TiO_2, (B) phase junction between α and β phase Ga_2O_3. *Reprinted (adapted) with permission from Zhang, J.; Xu, Q.; Feng, Z.; Li, M.; Li, C.* Angew. Chem. Int. Ed. ***2008***, 47, *1766–1769. Copyright (2008) Wiley-VCH and permission from Wang, X.; Xu, Q.; Li, M. R.; Shen, S.; Wang, X. L.; Wang, Y. C.; Feng, Z. C.; Shi, J. Y.; Han, H. X.; Li, C.* Angew. Chem. Int. Ed. ***2012***, 51, *13089–13092. Copyright (2012) Wiley-VCH.*

photocatalysis, the phase transformation of TiO_2 was systematically investigated *(70)*. For the small particles (< 60 nm), phase transformation to rutile nucleates at the interfaces of anatase grains. On the contrary, for the large particles (> 60 nm), the free surface, interface, and bulk of anatase TiO_2 can all function as rutile nucleation sites. Photocatalytic H_2 production on different composites of anatase and rutile has been found to be closely related to its surface-phase structure *(71)*. The formation of phase junctions between anatase and rutile TiO_2 provides a smooth path for photogenerated charge separation, which is regarded as the main factor for the highly photocatalytic activity of anatase and rutile mixed phased TiO_2 photocatalyst (Fig. 9A). It was reported that the phase transformation of TiO_2 from anatase to rutile can be restrained by surface modification with Na_2SO_4; when the

content of SO_4^{2-} in TiO_2 was increased, the ratio of anatase/rutile in the surface region was changed, and the SO_4^{2-} modified TiO_2 shows activities in H_2 production via photocatalytic reforming of methanol more than six times higher than pure phase samples, and the CO (undesired product) concentration in the produced H_2 was decreased by about two orders of magnitude *(72)*. Very recently, anatase–rutile phase junction was fabricated for photoelectrochemical water splitting, which showed superior performance in charge separation and transfer, achieving ca. 3 and 9 times photocurrent density enhancement compared to bare anatase and rutile TiO_2 electrodes, respectively, demonstrating the essential role of phase junction in photogenerated charge separation *(73)*.

Gallium oxide is an n-type semiconductor with several polymorph phases, including α and β phases. It was found that Ga_2O_3 with tunable α–β phase junctions can stoichiometrically split water into H_2 and O_2 with drastically enhanced activity compared with those of α or β phase structures (Fig. 9B) *(74)*. The samples with α phase or β phase alone have relatively low photocatalytic activities, whereas the sample with α–β phase junction shows much higher photocatalytic activity. High-resolution transmission electron microscopy (HRTEM) images clearly showed a well-defined α–β phase junction formed at the interface of α- and β phase Ga_2O_3, which accounts for the considerable enhancement of the photocatalytic activities of the α- and β mixed phase Ga_2O_3 based photocatalyst in overall water splitting. The kinetics of photogenerated charge carriers at α–β phase junction was also studied using ultrafast transient absorption spectroscopy (TAS) and time-resolved infrared (TR-IR) spectroscopy for understanding the role of phase junctions for photocatalytic water splitting (Fig. 10) *(74)*. It could be found that the presence of α–β phase junction results in an ultrafast electron transfer from α-Ga_2O_3 to β-Ga_2O_3 at approximately 3–6 ps, which is much faster than the recombination processes in the individual phases. This is why Ga_2O_3 photocatalyst with α–β phase junctions shows much more efficient charge separation than α and β phase Ga_2O_3. The lifetime of the long-lived photogenerated electrons of Ga_2O_3 with α–β phase junction is also found to be much longer than individual phases. Such long-lived electrons are most likely responsible for the enhancement of the photocatalytic activity. The energy alignment of band structures for different phases of Ga_2O_3 were also determined by calculating the energy levels of conduction and valence bands of α and β phase Ga_2O_3 confirming that the photogenerated charge separation is thermodynamically feasible for α–β phase junction.

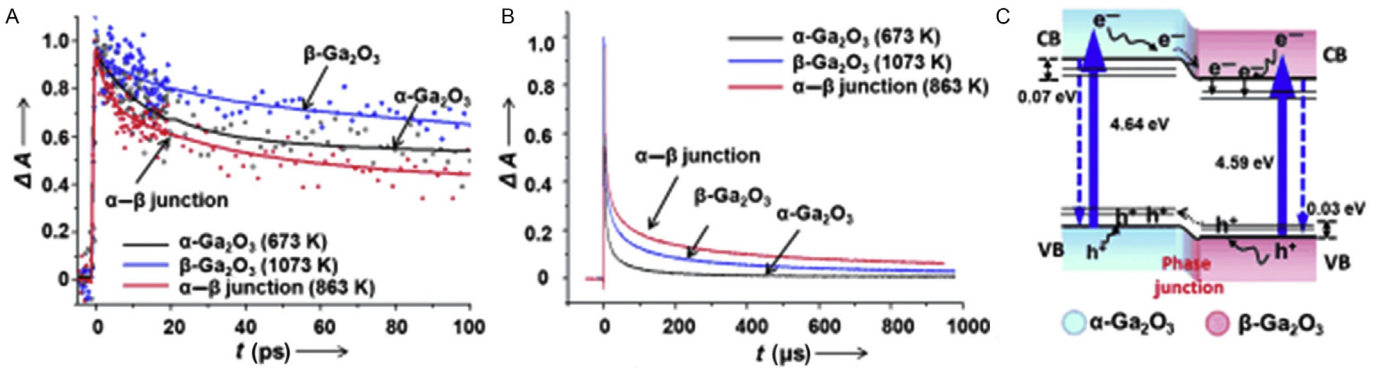

Fig. 10 The dynamics of photogenerated charge separation in phase junction of α and β phase Ga_2O_3. *Reprinted (adapted) with permission from Wang, X.; Xu, Q.; Li, M. R.; Shen, S.; Wang, X. L.; Wang, Y. C.; Feng, Z. C.; Shi, J. Y.; Han, H. X.; Li, C.* Angew. Chem. Int. Ed. ***2012***, 51, *13089–13092. Copyright (2012) Wiley-VCH.*

It should be noted that the unique property of phase junction for photogenerated charge separation is different from the general p–n junction and heterojunction formed between different semiconductors. The difference of band energy between phases is usually small, e.g., the calculated band gap difference between α and β phase Ga_2O_3 is about 0.1 eV. However, this tiny difference can indeed induce spatial separation of photogenerated electrons and holes at very short timescales, and the photocatalytic activity can be remarkably improved. Phase junction has been demonstrated to be a general strategy for photogenerated charge separation, e.g., α and β phase Bi_2O_3 *(75)*, hexagonal and monoclinic $BiPO_4$ *(76)*, α and β phase $Bi_4V_2O_{11}$ *(77)*.

6.1.3 Spatial Charge Separation in Semiconductor Crystal

Although some charge separation strategies have been demenstrated to be effective in composite semiconductor photocatalysts as discussed earlier, there are only a few examples focused on the development of charge separation strategy for a single semiconductor-based photocatalyst. Recently, spatial charge separation was found for a single crystal between its different exposed facets, e.g., $BiVO_4$ *(78)*. It was clearly observed that the photoreduction deposition of noble metals (Au, Pt, and Ag) selectively takes place on (010) facets of $BiVO_4$, while the photooxidation deposition of metal oxides (MnO_x and PbO_2) selectively appears on (110) facets of $BiVO_4$ (Fig. 11). These results unambigously indicate that the photogenerated electrons and holes are separated in space, and distribute on {010} and {110} facets, respectively. Single-particle fluorescence imaging also confirms this result using APF (3′-(*p*-aminophenyl) fluorescein) as the oxidation probe molecules *(79)*. Fig. 11D shows the fluorescence spectrum of APF solution with and without $BiVO_4$ under the light irradiation. The bright fluorescence areas due to oxidation of APF probe molecules by the holes nearby serve as the indication of the hole accumulating sites. In good agreement with the photodeposition results, photooxidation of APF molecules was only observed on the {110} facets of $BiVO_4$ crystal. The above results confirm the fact that the photogenerated electrons and holes can be separated to different facets of $BiVO_4$ single crystal under visible light irradiation. This is a unique demonstration of efficient charge separation on a single semiconductor crystal, which is different from "junction" strategies for charge separation. For the charge separation by "junction," the photogenerated electrons and holes are separated by the driving force such as built-in electric field in the depletion layer.

To investigate the driving force of spatial charge separation between different facets of semiconductor crystals, Kelvin probe force microscopy

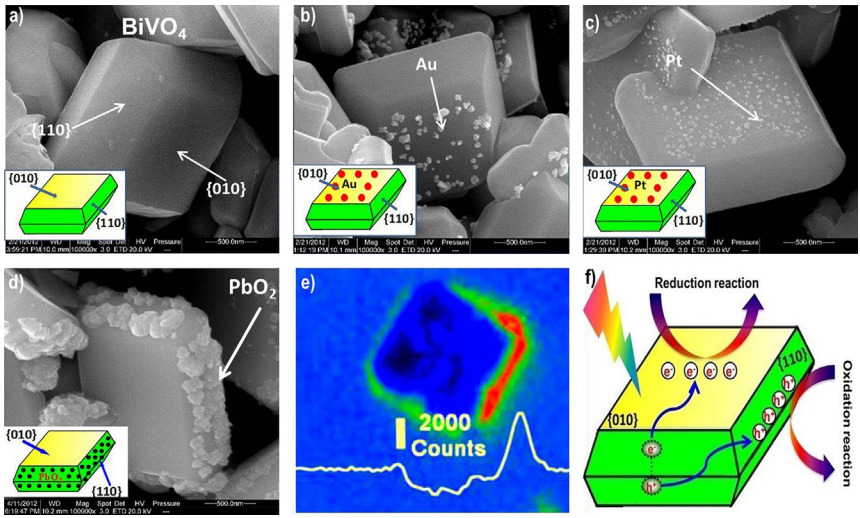

Fig. 11 Photogenerated charge separation between different facets of $BiVO_4$ crystals. *Reprinted (adapted) with permission from Li, R. G.; Zhang, F. X.; Wang, D. G.; Yang, J. X.; Li, M. R.; Zhu, J.; Zhou, X.; Han, H. X.; Li, C.* Nat. Commun. ***2013***, 4, *DOI:10.1038/ncomms2401. Copyright (2013) Nature Publishing Group and permission from Zhu, J.; Fan, F. T.; Chen, R. T.; An, H. Y.; Feng, Z. C.; Li, C.* Angew. Chem. Int. Ed. ***2015***, 54, *9111–9114. Copyright (2015) Wiley-VCH.*

(KPFM) and spatial-resolved surface photovoltage spectroscopy (SRSPV) were employed to investigate photogenerated charge separation between different facets of $BiVO_4$ crystal *(79)*. In KPFM experiments, the contact potential difference (CPD) between tip and sample can be used as the indication of the upward band bending as it is closely related to the surface potential induced by space charge region near the surface. As shown in Fig. 12, the SPV signal intensity on the {110} facet is 70 times stronger than that on the {010} facet, indicating that the band bending induced by the built-in electric field in the surface charge region of {110} facet is much bigger than that on the {010} facets, which is a strong support that the photogenerated holes are more preferred to be accumulated on {110} facet. It demonstrates that the surface band bending induced by the surface charge region is possible to be responsible for the observed spatial charge separation.

For the intrinsic reasons of such complicated spatial charge separation between different facets, there are some contradictory explanations to illustrate the results obtained on TiO_2 photocatalyst crystals with specific facets. For instance, based on the DFT simulation of surface properties of different facets, Pan et al. reported that the different photocatalytic activities of {001}, {010}, and {110} facets of anatase TiO_2 crystals are due to their surface and

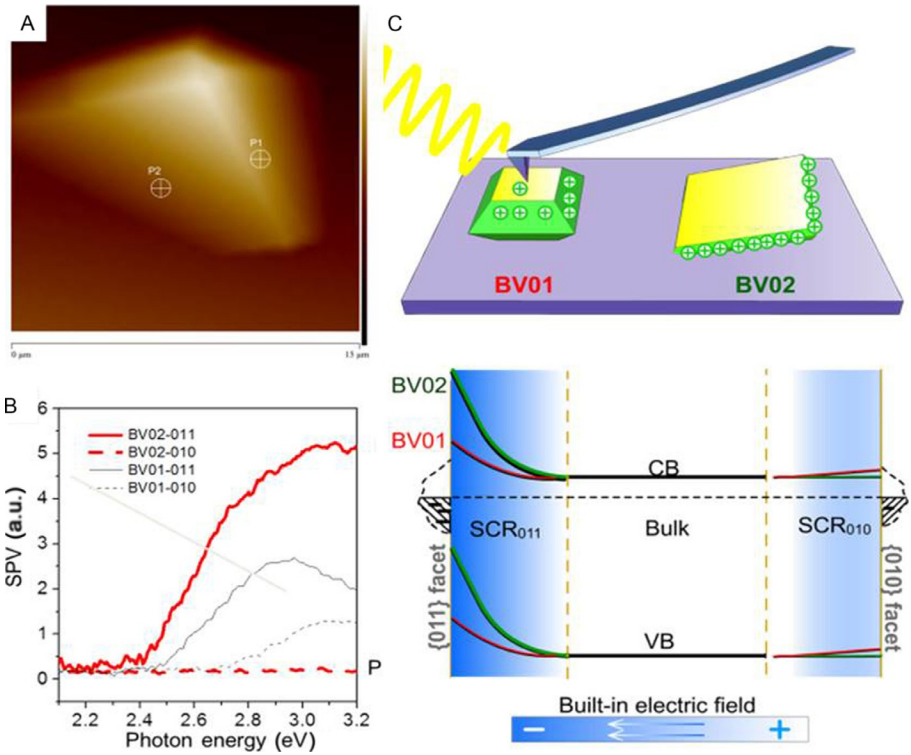

Fig. 12 Spatial-resolved surface photovoltage spectroscopy (SRSPV) of $BiVO_4$ crystals. *Reprinted (adapted) with permission from Zhu, J.; Fan, F. T.; Chen, R. T.; An, H. Y.; Feng, Z. C.; Li, C.* Angew. Chem. Int. Ed. ***2015***, 54, *9111–9114. Copyright (2015) Wiley-VCH.*

electronic structures *(80)*. Zheng et al. found a synergetic effect between well-defined {001} and {101} facets of a TiO_2 crystal, and the photogenerated charge separation can be enhanced by coexposing both crystal facets *(81)*. Yu et al. proposed that "surface heterojunction" formed between {001} and {101} facets of anatase TiO_2 crystal is responsible for its superior performance in photocatalytic CO_2 reduction *(82)*. However, all of these results just show the possible model to expain the experiment phonomeon but still lack of direct evidences for demenstrating them. Although the discussion of why spatial charge separation takes places between different facets is still ongoing, the investigations of photocatalytic reactions on semiconductor-based crystals are attracting more attention as many advanced characterization techniques for charge separation studies are developed rapidly.

More semiconductor crystals with spatial charge separation property have been explored (e.g., Cu_2WS_4 *(83)*, $PbTiO_3$ *(84)*, TiO_2 *(85,86)*, BiOCl

(87), and $La_5Ti_2CuS_5O_7$ *(88)*), and the spatial charge separation between facets is demonstrated to be general for many kinds of semiconductors. Up to now, spatial charge separation between facets has been well recongnized as a unique but general strategy for the design and preparation of semiconductor photocatalysts.

6.2 Dynamics of Photogenerated Charge Carriers

Investigating the dynamic behavior of photogenerated charge carriers is important for understanding the mechanism of photocatalytic water-splitting systems. Ultrafast spectroscopies, e.g., time-resolved photoluminescence spectroscopy (TR-PL), time-resolved infrared spectroscopy (TR-IR), and transient absorption spectroscopy (TAS), are powerful techniques to study the dynamics of photogenerated charge carriers. TR-PL can probe the radiation recombination of photogenerated charges, while TAS gives the absorption signal of photoinduced electrons and holes, and TR-IR can provide the dynamics of long-lived photogenerated charges *(89)*. Comprehensive using of these ultrafast spectroscopy could provide useful information on the fate of the photogenerated charge carriers in photocatalytic water-splitting processes. Taking $LaTaO_2N$ photocatalyst as an example, it was reported that $LaTaO_2N$ photocatalyst modified with CoO_x cocatalyst exhibits a high AQE of ~27% at 440 nm *(90)*. Such high AQE was ascribed to the efficient charge separation resulting in electrons with lifetime in the timescale of ~1 s. Femtosecond diffuse reflectance spectroscopy provides the evidence for the existence of energetically distributed trapped states in $LaTiO_2N$ *(91)*. It was found that the loading of CoO_x cocatalyst greatly affects the kinetics of charge separation only when the presence of excess energy (for band gap excitation) results in the generation of surface charges. Very recently, time-resolved visible to mid-IR absorption and emission spectroscopy was applied to investigate the behavior of photogenerated charge carriers in $SrTiO_3$ doped with transition metals (Ni, Ta) *(92)*. The results showed that codoping of Ni and Ta enhances photocatalytic activity under visible light irradiation but decreases the activity under UV light irradiation. The time-resolved spectroscopy result showed that doping of transition metals extended the lifetime of photogenerated charge carriers but decreased the reactivity of photogenerated electrons. Since overall photocatalytic activity is determined by competition between recombination and charge separation to the reactant molecules, the deactivation of the electron-consuming reaction is responsible for the decrease in overall photocatalytic activity. To know the intrinsic

roles of heterojunction for photogenerated charge separation, the dynamics of photogenerated charge carriers in $WO_3/BiVO_4$ heterojunction photoanodes has been studied by ultrafast TAS *(93)*. It was found that the better performance of $WO_3/BiVO_4$ heterojunction electrodes is a consequence of electron injection from $BiVO_4$ into WO_3, followed by back electron transfer from WO_3 to the holes in $BiVO_4$. The quick electron transfer driven by the built-in electronic field of heterojunction results in higher charge separation efficiency and consequently leads to better photocatalytic activity.

7. COCATALYSTS AND SURFACE CATALYTIC REACTIONS

Proper cocatalysts loaded on the surface of semiconductor can accelerate the rate of photocatalytic reactions. The cocatalysts generally serve as the reaction sites to catalyze the surface reactions and are also found to promote the charge separation driven by the interfacial electric field formed between the cocatalyst and semiconductor. In the photocatalytic water splitting, two half reactions, namely, proton reduction and water oxidation reactions generally require the corresponding cocatalysts. When cocatalyst is deposited on the surface, a depletion layer is formed at the interface between cocatalyst and semiconductor. A built-in electric field induced by the depletion layer may provide a driving force for separation of the photogenerated electrons and holes to participate in the surface reduction and oxidation reactions. That is to say, a proper cocatalyst not only provides active sites for proton reduction and water oxidation reactions but also enhances the efficiency of photogenerated charge separation.

7.1 Dual-Cocatalysts in Photocatalysis

Suitable cocatalysts are indispensable for achieving high efficiency in photocatalyst systems for solar energy conversion. Generally, two functional cocatalysts (dual-cocatalysts), a reduction cocatalyst and an oxidation cocatalyst, are introduced for promoting both reduction and oxidation reactions, respectively (Fig. 13) *(94)*. For photocatalytic water-splitting reaction, reduction cocatalyst is used for promoting the rate of proton reduction to hydrogen while oxidation cocatalyst for water oxidation. The rate determining step of the entire reaction is usually determined by one of the half reactions with the slowest kinetics. The theoretical minimum Gibbs free energy required for a water-splitting reaction is 237 kJ/mol; however, in practice, much more energy is required to overcome the kinetic energy barriers for both reduction and oxidation reactions on the surface of

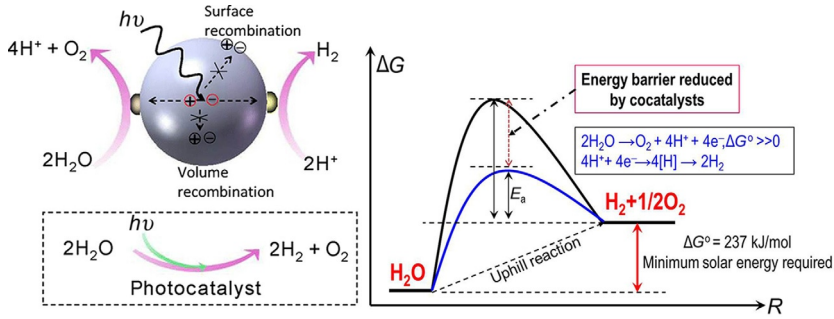

Fig. 13 Schematic description of the functions of cocatalysts and the intrinsic roles of dual-cocatalyst in lowering the activation energy in photocatalytic overall water splitting. *Reprinted (adapted) with permission from Yang, J. H.; Wang, D. G.; Han, H. X.; Li, C.* Acc. Chem. Res. ***2013***, 46, *1900–1909. Copyright (2013) American Chemical Society.*

photocatalyst. Particularly, water oxidation reaction usually requires much larger overpotential than proton reduction. Suitable cocatalysts can reduce such energy barriers by lowering the activation energy.

To realize an efficient overall photocatalytic reaction, both oxidation and reduction reactions are equally important. It has been widely demonstrated that coloading of both reduction and oxidation cocatalysts on the light harvesting semiconductor can greatly improve the photocatalytic activity for H_2 or O_2 production half reactions and overall water-splitting systems. A representative example for demonstrating the essential role of dual-cocatalysts is Pt–PdS/CdS photocatalyst reported in 2009 *(95)*. As shown in Fig. 14A, the photocatalytic H_2 production of CdS was enhanced remarkably by loading Pt or PdS cocatalyst. Interestingly, the photocatalytic activity was further enhanced to more than 300 times, when Pt and PdS are coloaded on CdS, corresponding to a measured AQE of 93% at 420 nm. The simultaneous existence of PdS acting as an oxidation cocatalyst and Pt acting as a reduction cocatalyst is supposed to be beneficial for efficient separation and transfer of the photogenerated electrons and holes, leading to the extremely high AQE. Furthermore, the PdS can also protect CdS from photocorrosion, making the PdS/CdS and Pt–PdS/CdS very stable under the photocatalytic reaction conditions. Another good example is Rh/Cr_2O_3–Mn_3O_4/GaN:ZnO photocatalyst, in which Rh/Cr_2O_3 acts as reduction cocatalysts for hydrogen production, while Mn_3O_4 acts as oxidation cocatalyst for water oxidation (Fig. 14B) *(96)*. When both Rh/Cr_2O_3 and Mn_3O_4 were simultaneously deposited on GaN:ZnO, photocatalytic overall water-splitting activity is improved significantly, demonstrating

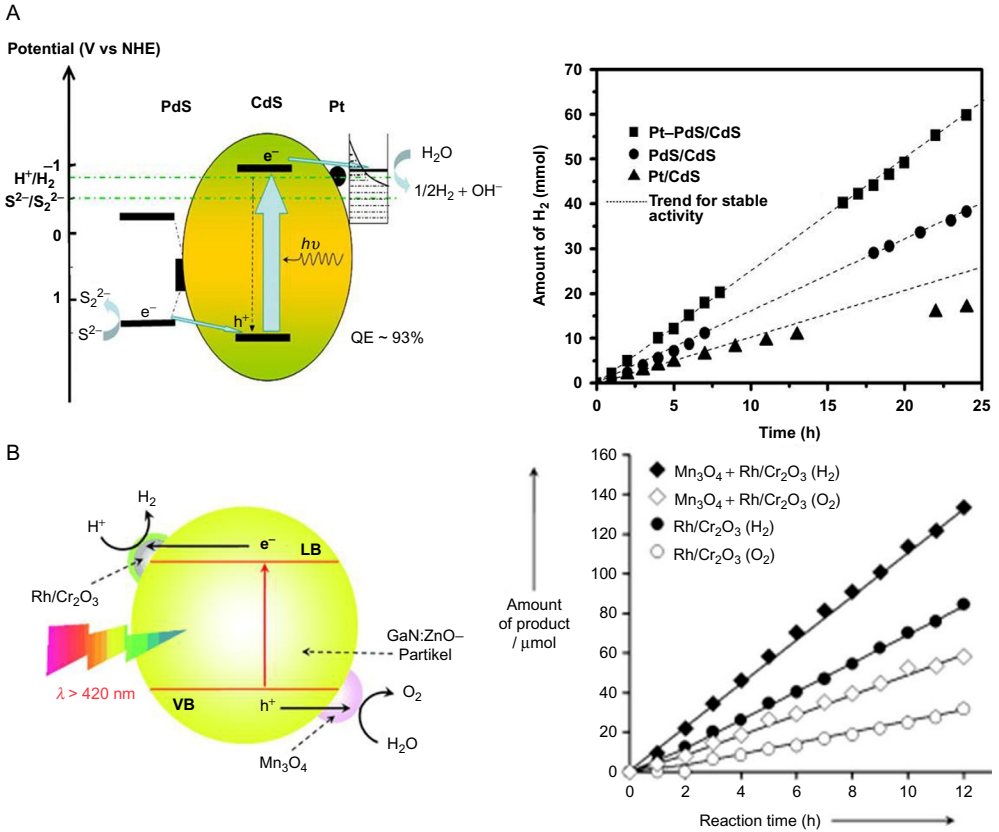

Fig. 14 Schematic model of dual-cocatalyst systems for photocatalytic water splitting. (A) Pt–PdS/CdS and (B)Rh/Cr_2O_3-Mn_3O_4/GaN:ZnO. *Reprinted (adapted) with permission from Yan, H. J.; Yang, J. H.; Ma, G. J.; Wu, G. P.; Zong, X.; Lei, Z. B.; Shi, J. Y.; Li, C.* J. Catal. ***2009***, 266, *165–168. Copyright (2009) Elsevier and permission from Maeda, K.; Xiong, A. K.; Yoshinaga, T.; Ikeda, T.; Sakamoto, N.; Hisatomi, T.; Takashima, M.; Lu, D. L.; Kanehara, M.; Setoyama, T.; Teranishi, T.; Domen, K.* Angew. Chem. Int. Ed. ***2010***, 49, *4096–4099. Copyright (2010) Wiley-VCH.*

the essential roles of dual-cocatalysts for promoting overall water splitting reaction.

The effect of dual-cocatalysts for both reduction and oxidation reactions in photocatalysis has been demonstrated in many photocatalyst systems. Zn_2GeO_4 coloaded with noble metals (Pt, Pd, Rh, Au) acting as reduction cocatalyst and metal oxides (RuO_2, IrO_2) acting as oxidation cocatalyst was reported to show a considerably synergistic effect on photocatalytic overall water splitting *(97)*. It was revealed that the photocatalytic activities of dual-cocatalysts modified Zn_2GeO_4 samples are much higher than those loaded with only reduction or oxidation cocatalyst, and even higher than the sum of the two individual ones. Lin et al. also extended the dual-cocatalyst concept to Pt–RuO_2/$BiVO_4$ photocatalyst for photocatalytic oxidation of thiophene using molecular O_2 as the electron acceptor; in this case, thiophene is oxidized on the surface of RuO_2 cocatalyst, while the reduction of O_2 to O_2^- takes place on Pt particles *(98)*.

The location of dual-cocatalysts on semiconductor surface were also found to be important in photocatalysis. The reduction and oxidation cocatalysts should be deposited on the right sites (reduction cocatalysts on the electron-accumulating sites and oxidation cocatalyst on the hole-accumulating sites) so that the photogenerated electrons and holes can be trapped for surface catalytic reactions. It is obvious that the recombination of electrons and holes easily takes place when they are trapped by the cocatalysts when they are located on the wrong sites (e.g., reduction cocatalysts on the hole-accumulating sites and/or oxidation cocatalysts on the electron-accumulating sites). The cocatalysts were often deposited by impregnation or adsorption method as the preparation for thermal catalysts, in which the cocatalysts are radomly distributed on the surface. However, based on the spatial charge separation between facets of semiconductor crystals mentioned before, it is possible to deposit the reduction and oxidation cocatalysts separately on electron-accumulating and hole-accumulating facets by in situ photodeposition method *(99)*. Fig. 15 shows the scheme for depositing proper cocatalysts on the right sites of $BiVO_4$ crystal by spatial charge separation strategy. When the reduction cocatalyst (Pt) and oxidation cocatalyst (Co_3O_4) are randomly deposited on every facet of $BiVO_4$ by impregnation method, the photocatalytic performance is rather low. Meanwhile, a remarkable synergetic effect of dual-cocatalysts was achieved when the dual-cocatalysts are selectively deposited on the different facets by photodeposition method, the photocatalytic activity can be enhanced to more than 100 times of that of bare $BiVO_4$ and more than 10 times of that with

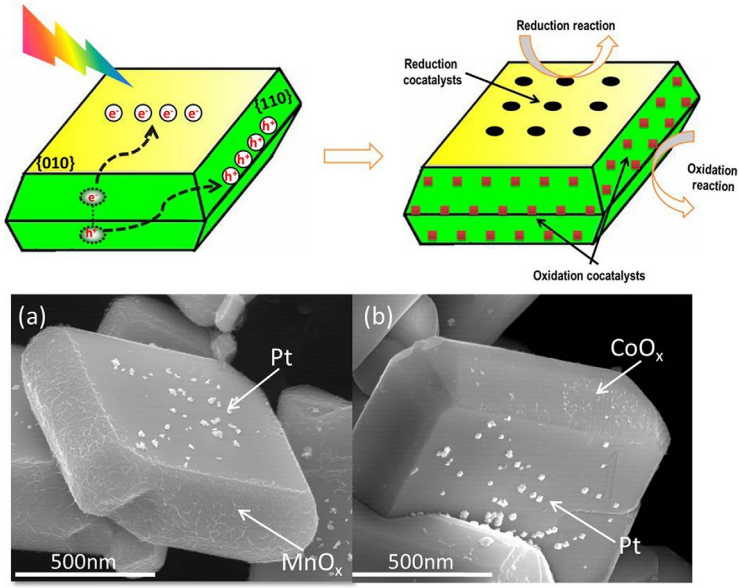

Fig. 15 Selective deposition of reduction and oxidation cocatalysts on different facets based on the spatial charge separation on $BiVO_4$ crystal. *Reprinted (adapted) with permission from Li, R. G.; Han, H. X.; Zhang, F. X.; Wang, D. G.; Li, C.* Energy Environ. Sci. ***2014**, 7, 1369–1376. Copyright (2014) Royal Society of Chemistry.*

dual-cocatalysts randomly distributed. In this case, photogenerated electrons and holes can be efficiently trapped by the reduction and oxidation cocatalysts once transferred to the surface. These results clearly indicate the advantage of rational deposition of dual-cocatalysts on the right sites by the photodeposition strategy based on the spatial charge separation between different facets. Following this strategy, Zhang et al. found that the reduction and oxidation cocatalysts can be separately deposited on the plane and edge of BiOCl nanoplates, which can greatly enhance the photocatalytic activity *(87)*. BiOCl is usually not stable due to its photoreduction by photogenerated electrons during photocatalytic reactions. However, by selective deposition of dual-cocatalysts on the different facets, the stability of BiOCl was improved from 3 h to more than 30 h. All these examples clearly indicate that the rational deposition of the dual-cocatalysts on the right sites of photocatalyst is effective for solar energy conversion.

The spatial separation of reduction and oxidation cocatalysts onto different surface sites is also important for accelerating the catalytic reactions by avoiding possible reverse reactions. The spatial charge separation between

facets are also documented in the literature for the separation of active sites. For example, introduction of intrinsic electronic field (e.g., ferroelectric field by spontaneous electric polarization in the bulk of ferroelectric semiconductor) can induce the spatial separation of photogenerated charges and dual-cocatalysts. It was reported that the reduction and oxidation active sites can be separately assembled on $PbTiO_3$ photocatalyst induced by the ferroelectric field in the bulk regardless of its morphologies as nanoplates *(84)* or irregular shapes *(100)*. Such kind of internal electric field in the bulk of photocatalyst may influence the separation of photogenerated electrons and holes and further spatial separation of active sites for surface catalytic reactions.

7.2 Relation Between Cocatalysts in Photocatalysis and Electrocatalysis

Electrocatalysis is a catalytic process involving oxidation and reduction reactions through the direct transfer of electrons, which requires electrocatalysts to lower the overpotential of the reactions. An electrocatalyst can accomplish the surface catalytic reaction through different reaction pathways with different thermodynamic potentials. A good electrocatalyst can maximally reduce the overpotential required for driving a specific electrochemical reaction. The process of surface catalytic reactions in photocatalysis is very similar to electrocatalysis. In principle, nanoparticle photocatalyst can be considered as an integrated microelectrochemical cell, in which the reduction reaction sites (e.g., H_2 evolution sites) are the cathodes, while the oxidation reaction sites (e.g., O_2 evolution sites) are the anodes *(101)*. The difference of the two similar processes is that the reduction and oxidation reactions are separated onto different electrodes or not.

Fig. 16 schematically describes the role of cocatalysts in photocatalytic and photoelectrochemical water splitting. By loading proper cocatalysts on the surface of photocatalyst, the photocatalytic activities can be significantly enhanced, indicating that cocatalyst decreases the activation energy (E_a) of photocatalytic water splitting. In photoelectrochemical water splitting, overpotential needs to be overcome for the electrocatalytic reactions. The electrocatalyst on the surface of photoanode can trap the photogenerated charges, provide the active sites, and accelerate the surface reactions, resulting in an enhancement of the photocurrent density and a negative shift of onset potential. The negative shift of onset potential corresponds to lowering the overpotential of reactions. Therefore, we have

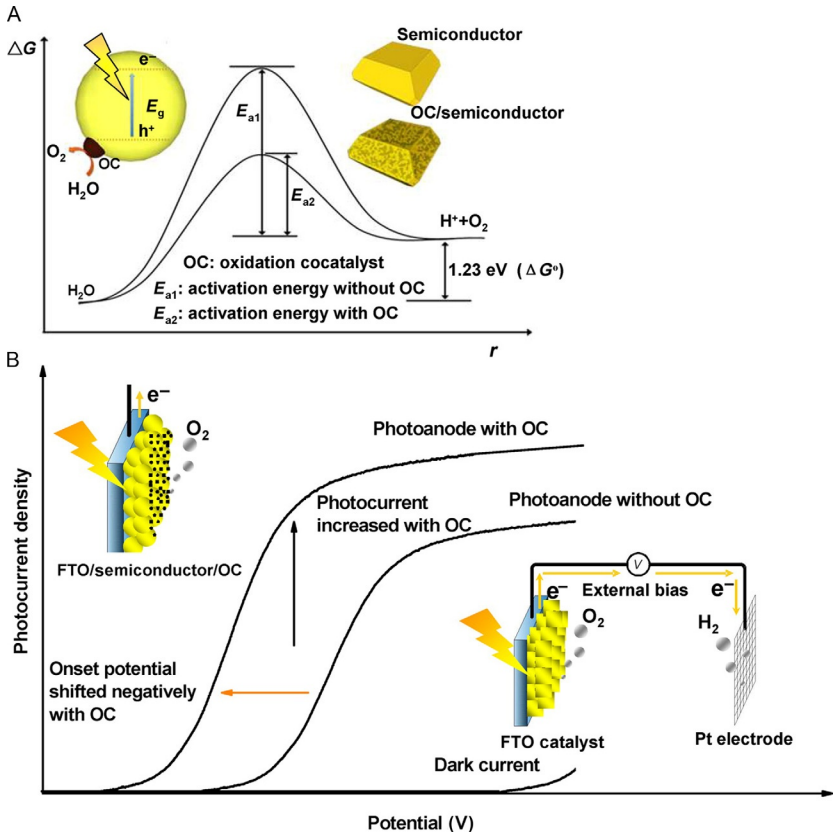

Fig. 16 Schematic description of the role of oxidation cocatalyst in (A) photocatalytic water oxidation and (B) PEC water oxidation, respectively. *Reprinted (adapted) with permission from Yang, J. H.; Wang, D. G.; Han, H. X.; Li,C. Acc. Chem. Res. 2013, 46, 1900–1909. Copyright (2013) American Chemical Society.*

deduced the following energy relations for photocatalysis and photoelectrocatalysis in water oxidation reaction,

$$\text{photocatalysis}: E \geq E_g + E_a \tag{12}$$

$$\text{photoelectrocatalysis}: E \geq E_g + E_{AOP} \tag{13}$$

where E is the minimum energy required for the water splitting reaction to take place, E_g is the band gap energy of light-harvesting semiconductor, E_a is the activation energy in photocatalysis, and E_{AOP} is the activation overpotential.

In photoelectrochemical water oxidation, the activation overpotential is essentially related to the activation energy in photocatalysis when the same

semiconductor is used for both processes, namely, $E_a \sim E_{AOP}$. For overall water splitting, the activation energy should basically consider both of the half reactions, proton reduction and water oxidation. Water oxidation reaction usually dominates the activation energy of the overall water splitting because it is a more challenging reaction due to its multistep, four-electron and four-proton transferring process. The efficient electrocatalyst may serve as cocatalysts in photocatalysis, and many water oxidation cocatalysts have been screened from electrocatalysts. For example, CoPi has been widely used as an active water oxidation electrocatalyst in the early days in electrolysis of water; nowadays many examples have demonstrated that CoPi can serve as efficient water oxidation cocatalyst in photocatalysis. For example, when CoPi was deposited on $BiVO_4$ photoelectrode, a remarkable negative shift of photocurrent onset potential was observed, suggesting that less electric energy is required for photoelectrochemical water oxidation *(101)*. Apparently, loading of CoPi on $BiVO_4$ electrode can lower E_{AOP} for photoelectrochemical water oxidation as consequence of lowering the E_a of water oxidation reaction. Lowering the activation energy to promote the water oxidation reaction by using electrocatalysts as cocatalysts has also been confirmed by loading various electrocatalysts (CoPi, CoO_x, IrO_2, MnO_x, etc.) on the surface of $BiVO_4$ (Fig. 17). The photocatalytic water oxidation performance and the photocurrent density were found to follow the same order in photocatalytic and photoelectrochemical water-splitting reactions, which indicates the close relation between cocatalyst in photocatalysis and electrocatalyst in photoelectrocatalysis *(101)*.

7.3 Surface Reactions on Cocatalysts

As cocatalysts provide active sites for surface catalytic reactions, the chemical properties of cocatalyst (structure, species, location, etc.) affect the behavior of surface reactions. Several typical examples were chosen to illustrate how these factors influence on the catalytic reactions in photocatalytic water splitting.

In photocatalytic overall water splitting, the reverse reaction of H_2 and O_2 to form H_2O ($2H_2 + O_2 = 2H_2O$), which inevitably decelerates the photocatalytic activity and should be avoided as much as possible. Generally, noble metals provide active sites for proton reduction for H_2 evolution, meanwhile they may also serve as sites for activation of H_2 so that the reverse reaction is accelerated. To suppress the reverse reaction in photocatalytic water splitting on $(Ga_{1-x}Zn_x)(N_{1-x}O_x)$ photocatalyst, a core/shell

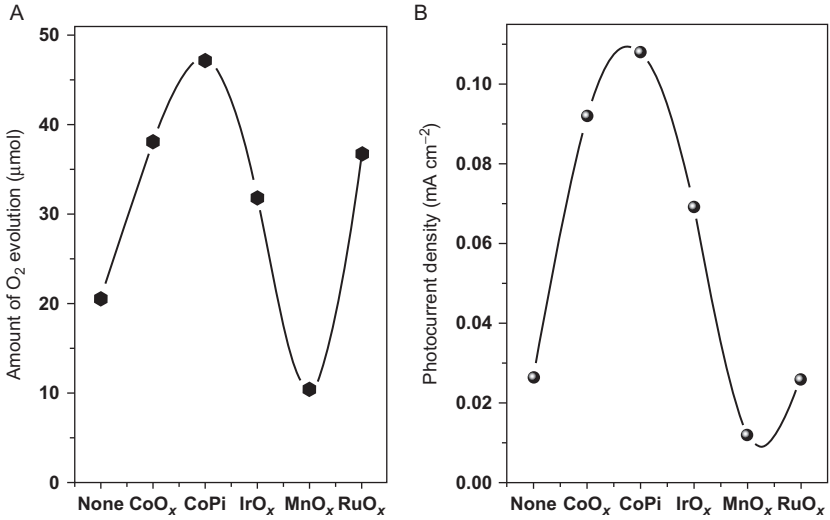

Fig. 17 The correlation between photocatalytic and photoelectrochemical water oxidation on different cocatalysts-loaded $BiVO_4$. *Reprinted (adapted) with permission from Wang, D. E.; Li, R. G.; Zhu, J.; Shi, J. Y.; Han, J. F.; Zong, X.; Li, C.* J. Phys. Chem. C ***2012***, 116, 5082–5089. *Copyright (2012) American Chemical Society.*

structured cocatalyst, M/Cr_2O_3 (M = Rh, Pt, Pd, Ir, etc.), was designed and fabricated (Fig. 18) *(102–105)*. The Cr_2O_3 layer is permeable to protons and the evolved hydrogen molecules, but not to oxygen. After coating a thin layer of Cr_2O_3 on noble metals to form a core/shell structure, the overall water-splitting activity can be greatly enhanced. However, the bare Cr_2O_3 on the $(Ga_{1-x}Zn_x)(N_{1-x}O_x)$ photocatalyst is not active for overall water splitting. When noble metals (e.g., Rh) were covered with Cr_2O_3 shell, the rates of H_2 and O_2 evolution are drastically increased because of the suppression of reverse reaction. The suppression was attributed to a tunneling mechanism that allows photogenerated electrons to migrate first to the surface of noble metal and then to the outer oxide surface prior to hydrogen evolution. Besides, spatially separate the reduction and oxidation active sites on the surface of photocatalyst may also reduce the collision probability of involved H_2 and O_2 to suppress the reverse reaction *(20)*.

The species of redox cocatalysts on the surface of semiconductor also play significant roles in photocatalytic water-splitting process. Taking NiO_x-loaded $SrTiO_3$ photocatalyst as an example, Townsend et al. employed a surface voltage spectroscopy as a useful tool to study the photoinduced charge transfer processes and found that NiO_x cocatalyst is actually composed of both metallic and oxides nickel states, metallic Ni serves as an

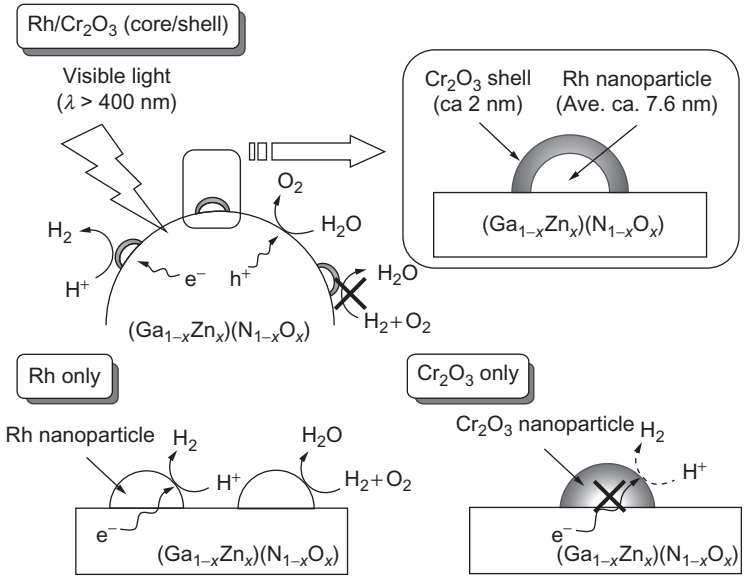

Fig. 18 The mechanism of M/Cr_2O_3 core/shell nanoparticles as a cocatalyst for photocatalytic overall water splitting. *Reprinted (adapted) with permission from Maeda, K.; Teramura, K.; Lu, D. L.; Saito, N.; Inoue, Y.; Domen, K.* Angew. Chem. Int. Ed. ***2006***, 45, *7806–7809. Copyright (2006) Wiley-VCH.*

electron trapping site (site for proton reduction) and NiO as a hole trapping site (site for water oxidation) (Fig. 19) *(106)*. Electrochemical measurements showed that the overpotential for water oxidation well correlates with the NiO content, whereas the overpotential for water reduction depends on the Ni content. Probe of the charge enrichment sites by photodeposition experiments with $NiCl_2$ and H_2PtCl_6 on $NiO/SrTiO_3$ provides an evidence that electrons are available on the $SrTiO_3$ surface rather than on the NiO particles. All of the above results demonstrate an alternative mechanism, in which the NiO particles function as a water oxidation cocatalyst and the Ni particles as a water reduction cocatalyst, revealing the critical role of dual-cocatalysts in photocatalytic water splitting.

The variation of redox cocatalyst species induced by photogenerated electrons or holes during photocatalyitc reactions were also observed to be correlated with photocatalytic activities. Zhang et al. studied the role of NiO_x cocatalyst for overall water splitting using $NaTaO_3$ as photocatalyst *(107)*. They found that although NiO was solely deposited on the surface of $NaTaO_3$ by impregnation method, the existence of both metallic Ni and NiO were observed during photocatalytic reaction, and

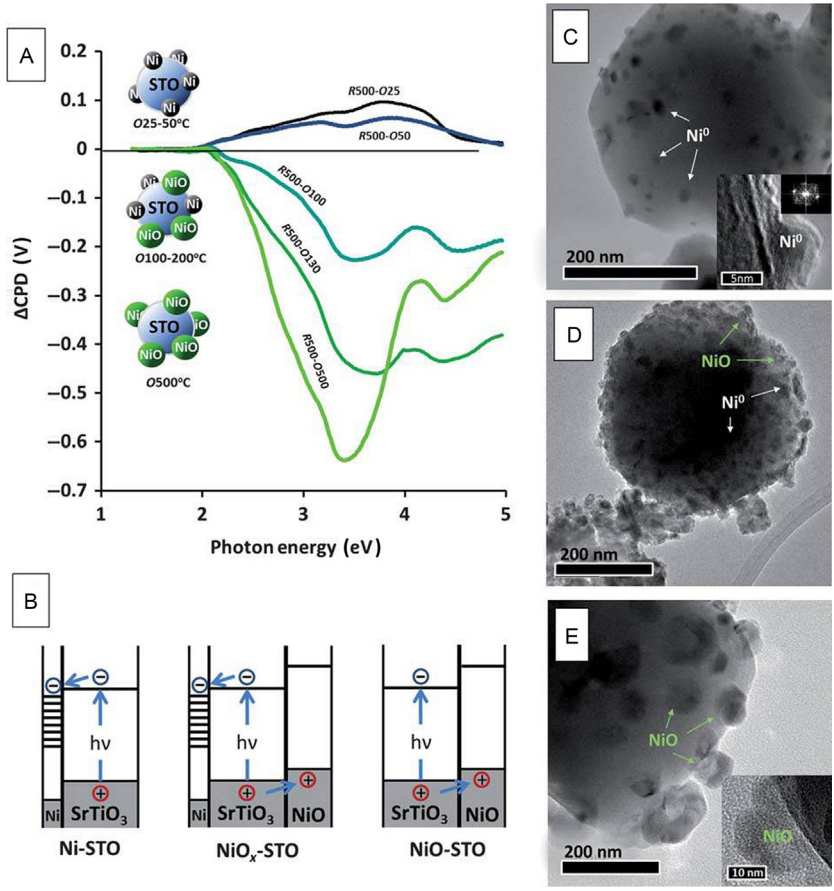

Fig. 19 Light-induced contact potential change (ΔCPD) of NiO-$SrTiO_3$ by controlling oxidation state via heating in air at different temperatures. *Reprinted (adapted) with permission from Townsend, T. K.; Browning, N. D.; Osterloh, F. E.* Energy Environ. Sci. ***2012***, *5, 9543–9550. Copyright (2012) Royal Society of Chemistry.*

the actual roles of metallic Ni and NiO species for proton reduction and water oxidation respectively were confirmed by X-ray photoelectron spectroscopy and synchrotron X-ray absorption spectroscopy analysis (Fig. 20A). That is to say, the actual cocatalysts for overall water splitting on $NaTaO_3$ are metallic Ni and NiO, but not NiO itself. At the initial stages of reaction, the photogenerated electrons reduce partial of NiO to metallic Ni at reduction sites so that nonstoichiometric amounts of H_2 and O_2 were generated in the reaction system initially. As the reaction proceeds, the species of NiO and metallic Ni finally reach a balance to give

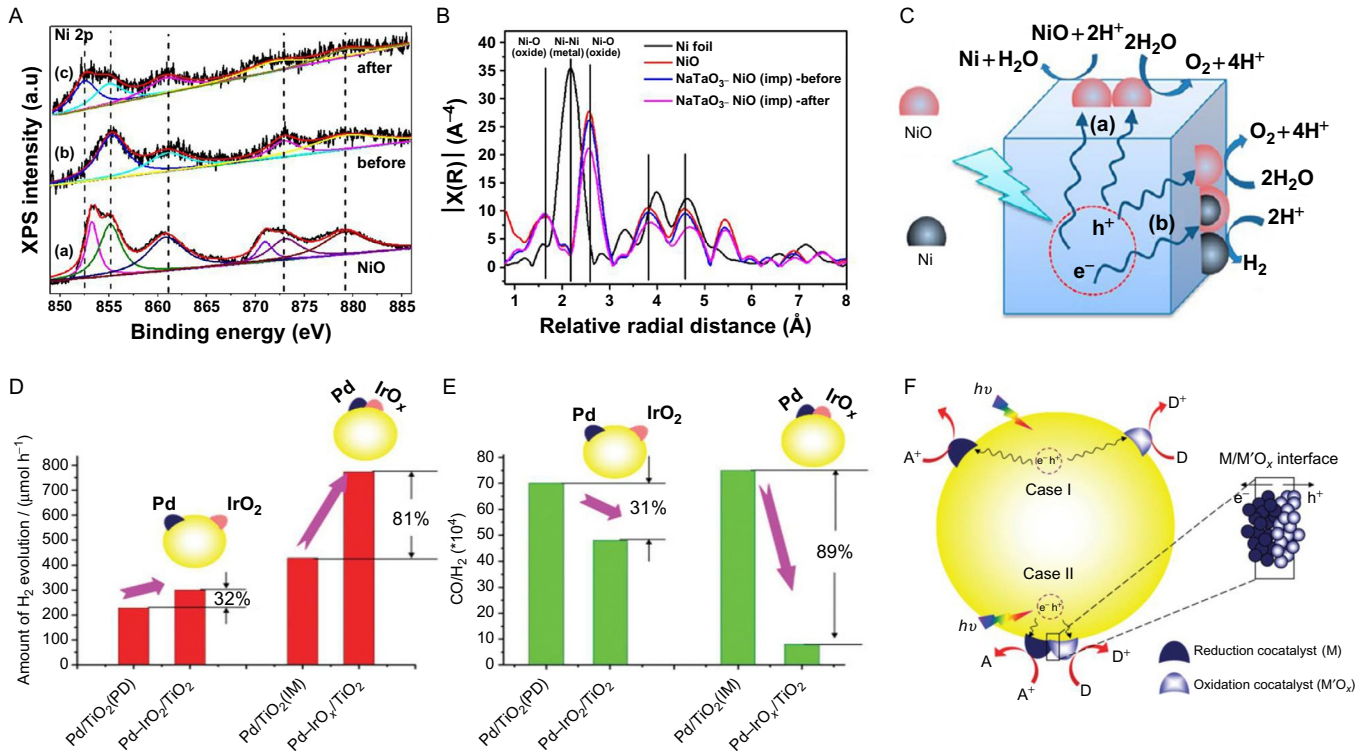

Fig. 20 (A–C) Intrinsic role of NiO_x cocatalyst on $NaTiO_3$ for overall water splitting. (D–F) Comparison of dual-cocatalysts with separated and intimately contacted for photocatalytic methanol reforming. *Panels (A–C) reprinted (adapted) with permission from Zhang, Q.; Li, Z.; Wang, S.; Li, R.; Zhang, X.; Liang, Z.; Han, H.; Liao, S.; Li, C.* ACS Catal. ***2016***, 6, *2182–2191. Copyright (2016) American Chemical Society; panels (D–F) reprinted (adapted) with permission from Ma, Y.; Chong, R.; Zhang, F.; Xu, Q.; Shen, S.; Han, H.; Li, C.* Phys. Chem. Chem. Phys. ***2014***, 16, *17734–17742. Copyright (2014) Royal Society of Chemistry.*

H_2 and O_2 evolution in stoichiometric ratio. The enhancement of the overall water-splitting activity is due to the synergetic effect between NiO and metallic Ni that in situ generated by photoexcited charges during the photocatalytic reaction.

The interaction between redox cocatalyst species also shows influences on catalytic reaction in photocatalysis. Ma et al. investigated the promotion effect of dual-cocatalysts on TiO_2 for photocatalytic methanol reforming and hydrogen production *(108)* and they found that intimate contact between the Pt (reduction cocatalyst) and IrO_2 (oxidation cocatalysts) can surprisingly lead to the enhancement of photocatalytic activity in H_2 production and sharp decrement of the CO/H_2 ratio (Fig. 20B). The interface between Pd and IrO_2 cocatalyst induces electrons and holes readily to be separated rather than serious recombination. When the dual-cocatalysts are closely contacted, the photogenerated charges in the surface skin region have a much shorter transportation distance to the surface and more photogenerated charges could be utilized for surface reactions. The interaction between intimately contacted dual-cocatalysts also affects the kinetics of catalytic reactions so that HCOOH could be totally oxidized to CO_2 but CO, leading a decrease of CO ratio in the final products.

7.4 Mechanism of Catalytic Reactions

Intensive researches have been paid on the development of visible light-responsive photocatalysts by controlling band structure, crystallinity, particle size, and morphology for improving the activity of photocatalytic water splitting. However, the reaction mechanism is still not quite well understood because the photocatalytic water-splitting reactions proceed through a complicated multistep process. In this section, taking the TiO_2-based photocatalyst as an example, the mechanism of photocatalytic water splitting will be briefly discussed.

In order to achieve a higher charge separation efficiency, the undesired and competing charge recombination should be minimized. However, the rate of charge recombination is usually in the same magnitude order of charge separation and transferring, leading to the fact that the majority of the charges cannot be utilized in the following catalytic reactions. For TiO_2-based photocatalyst, it has been generally recognized that more than 90% of photogenerated electrons and holes recombine within nanosecond timescale, which is much faster than the timescale of surface reactions. Tang and coworkers studied the kinetic process of photocatalytic water splitting,

especially water oxidation on TiO_2 using transient absorption spectroscopy *(109)*. Fig. 21 shows the quantum efficiency of O_2 evolution as a function of the photon number absorbed per nanoparticle using electron scavengers. Interestingly, the maximum quantum yield of photocatalytic water oxidation on TiO_2 photocatalyst occurs at an illumination intensity of four photons per particle. This is exactly what would be expected if the holes are not able to migrate between nanoparticles on the timescale of catalytic reaction. The result is the quantitative evidence of water oxidation for oxygen evolution driven by four photons and four electrons, which is reminiscent of the four-electron transfer water-splitting process in natural photosynthesis system.

In situ detection of reaction intermediates provides useful information for understanding the mechanism of photocatalyitc water splitting. Nakamura et al. introduced in situ multiple internal reflection infrared absorption spectroscopy to detect the primary intermediates of oxygen evolution reaction on rutile TiO_2 photocatalyst *(110)*. They found that two oxygen-containing species appeared at 838 and 812 cm^{-1} under the light irradiation in the presence of Fe^{3+} as electron acceptor, which could be assigned to the O–O stretching mode of surface peroxo species, TiOOH and TiOOTi, respectively via isotope labeling experiment. A mechanism

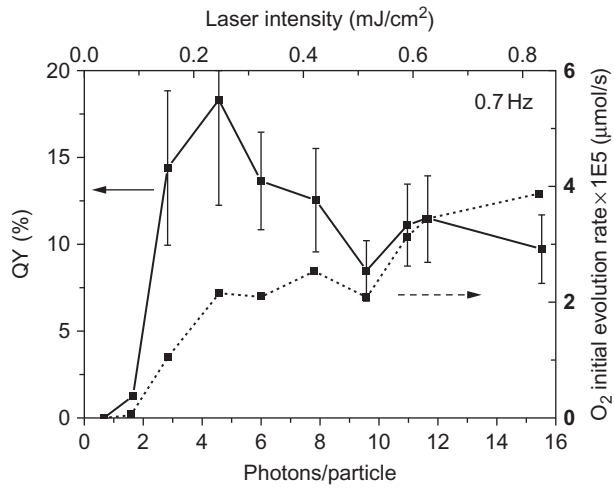

Fig. 21 Quantum yield and O_2 production rate as a function of excitation intensity expressed as photon number absorbed per pulse per TiO_2 particle. *Reprinted (adapted) with permission from Tang, J.; Durrant, J. R.; Klug, D. R.* J. Am. Chem. Soc. ***2008***, 130, *13885–13891. Copyright (2008) American Chemical Society.*

of water oxidation by photogenerated holes was then proposed based on the detected intermediates (Fig. 22). Frist, the reaction is initiated by a nucleophilic attack of H_2O molecule on a surface-trapped hole at a lattice O site to form [Ti–O·OH–Ti] radicals accompanied by Ti–O bond breaking, then two radicals [Ti–O·OH–Ti] coupled with each other to form surface peroxo species, TiOOTi. Such peroxo species was further oxidized by photogenerated holes and finally leads to oxygen evolution together with [Ti–O–Ti]. Li and coworkers found that the overall water-splitting performance, especially oxygen evolution of TiO_2 photocatalyst is attributed to both kinetics and thermodynamics *(17)*. Kinetically the process of photocatalysis differs on anatase and rutile TiO_2 because the reactions go through different intermediates ($^{\bullet}OH$ radical for anatase TiO_2 and peroxy species for rutile TiO_2). Thermodynamically, there are many trap states lying near the valence bands of anatase, which increase the overpotential of water oxidation; however, no or less trap states exist in rutile, which leads to less overpotential for water oxidation. After prolonged photoirradiation, these trap states were diminished and hence the overall water splitting for both hydrogen and oxygen evolution was observed.

As photocatalytic water oxidation for oxygen evolution is a complicated and challenging process, many theoretical scientists focus their interests on the simulation of such process to better understand the mechanism of photocatalytic water splitting. Valde´s and Nørskov et al. chose rutile TiO_2 (110) surface to investigate the kinetics of photocatalytic water oxidation process theoretically *(111)*. They assumed that the oxygen evolution reaction proceeds through one-by-one electron transfer steps as follows:

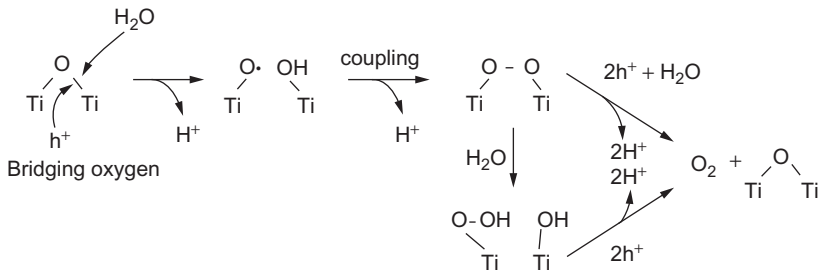

Fig. 22 Reaction scheme for the photocatalytic water oxidation on rutile TiO_2 surface. *Reprinted (adapted) with permission from Nakamura, R.; Nakato, Y.* J. Am. Chem. Soc. ***2004***, 126, *1290–1298. Copyright (2004) American Chemical Society.*

$$\text{Step 1}: H_2O + * \rightarrow HO^* + H^+ + e^-$$
$$\text{Step 2}: HO^* \rightarrow O^* + H^+ + e^-$$
$$\text{Step 3}: H_2O + O^* \rightarrow HOO^* + H^+ + e^-$$
$$\text{Step 4}: HOO^* \rightarrow O_2 + * + H^+ + e^-$$

* stands for the coordinatively unsaturated sites where the reaction takes place.

The surface structures and free energies of the intermediates for oxygen evolution reaction on the rutile TiO_2 (110) surface is shown in Fig. 23. The rate-limiting step, that is, the step with the highest Gibbs free energy change, corresponds to the step 1 when the first hole reacted with H_2O molecular to form HO*. Meanwhile, the most favored step is the last step, namely, the oxidation of HOO* to O_2 molecular for photocatalytic water oxidation

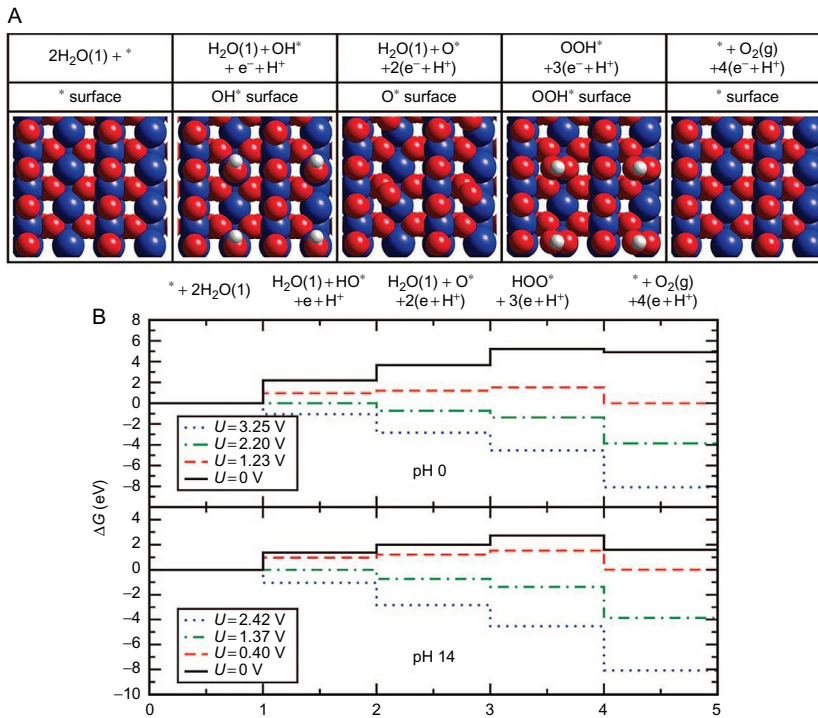

Fig. 23 Structures and free energies of the intermediates for oxygen evolution reaction on the rutile TiO_2 (110) surface. *Blue spheres*, metal ions; *red spheres*, oxygen; *white spheres*, hydrogen. *Reprinted (adapted) with permission from Valde´s, A.; Qu, Z.-W.; Kroes, G.-J.; Rossmeisl, J.; Nørskov, J. K.* J. Phys. Chem. C ***2008***, 112, *9872–9879. Copyright (2008) American Chemical Society.*

on TiO_2 photocatalyst. These theoretical calculation to accurately simulate the reaction processes and surface structures, together with advanced spectroscopy for detection of intermediates during photocatalytic reactions will be instructive and helpful for deeply understanding the mechanism of photocatalytic water splitting.

8. PHOTOCATALYSTS FOR OVERALL WATER SPLITTING

Constructing an efficient photocatalytic overall water splitting system should simultaneously consider many factors, e.g., light absorption, photogenerated charge separation, and proper cocatalysts for catalytic reactions. Photocatalysts capable for overall water splitting can be simply summarized into two primary approaches (Fig. 24). One approach is to split water into H_2 and O_2 using a single photocatalyst without any additional redox mediators. The other approach is to apply a two-step excitation process using two different photocatalysts as H_2-evolution and O_2-evolution photocatalysts coupled with an electronic redox mediator, which is principally similar to the Z-scheme charge separation process in natural photosynthesis system.

8.1 Single Photocatalyst System

Many single photocatalysts have been developed for overall water splitting and most of them have already been presented in Session 3. For example, NiO-loaded $NaTaO_3$ doped with La element possesses a nanostep structure on the surface for spatial separation of electrons and holes, which shows a high photocatalytic activity for water splitting with AQE of 56% at 270 nm *(24)*. Zn ion-doped Ga_2O_3 photocatalyst was prepared using dilute

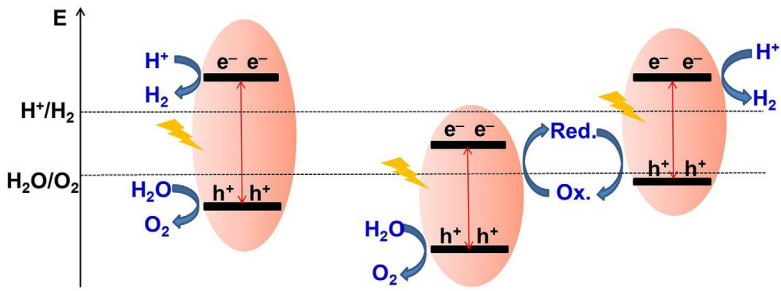

Fig. 24 Scheme of photocatalytic water splitting by single photocatalyst and Z-scheme of two-step photoexcitation photocatalyst systems.

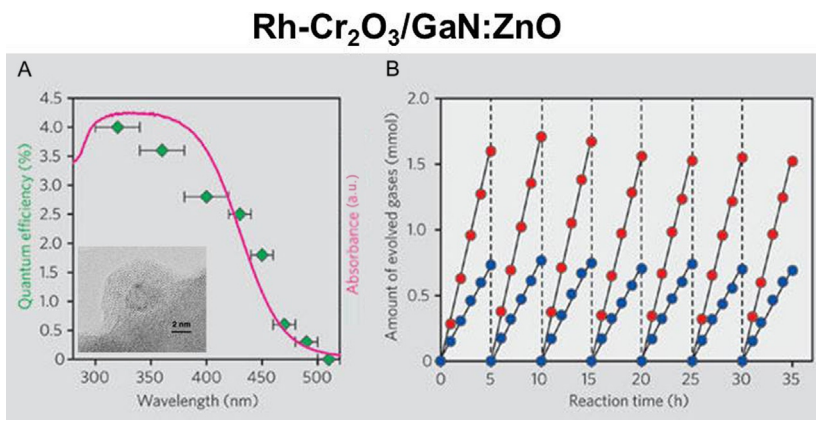

Fig. 25 Example of single photocatalyst, Rh-Cr_2O_3/GaN:ZnO, for photocatalytic overall water splitting. *Reprinted (adapted) with permission from Maeda, K.; Teramura, K.; Lu, D. L.; Takata, T.; Saito, N.; Inoue, Y.; Domen, K.* Nature, ***2006***, 440, *295–295. Copyright (2006) Nature Publishing Group.*

$CaCl_2$ solution, which reveals an extremely high AQE of 71% under irradiation at 254 nm *(112)*. Al-doped $SrTiO_3$ photocatalyst using $SrCl_2$ flux treatments showed an AQE of 30% at 360 nm in overall water-splitting reaction *(113)*. The representative visible light-responsive photocatalyst for overall water splitting is GaN:ZnO loaded with Rh/Cr_2O_3 cocatalyst (Fig. 25), which exhibits stable hydrogen and oxygen evolution activity and showed AQE as high as 5.9% at 420 nm *(102,114)*. Other photocatalysts for overall water splitting under visible light irradiation have also been widely explored, e.g., $In_{1-x}Ni_xTaO_4$ *(115)*, $LaMg_xTa_{1-x}O_{1+3x}N_{2-3x}$ *(116)*, nitrogen-doped graphene oxide quantum dots *(117)*, InGaN/GaN nanowire *(118)*). In spite of these progresses on overall water splitting in the past decades, the STH efficiency of photocatalytic water splitting using particulate photocatalyst is still relatively low (generally less than 1%) and far beyond the expectation for industrial demonstrations and applications.

8.2 Z-Scheme Photocatalyst System

In natural photosynthesis system, photogenerated charges are separated and transferred between photosystem II and photosystem I through a charge-transferring chain constituting the so-called Z-scheme reaction pathway. Learning from nature, mimicking such kind of functional Z-scheme process using reversible redox mediators and two photocatalysts (a H_2-evolution photocatalyst and an O_2-evolution photocatalyst) has been broadly studied.

Over the H_2-evolution photocatalyst, the photogenerated electrons reduce water to H_2 and the photogenerated holes oxidize mediator to an oxidation state. Then the oxidized mediator is reduced back by electrons generated on the O_2-evolution photocatalyst, where the photogenerated holes oxidize water to O_2. Such a two-step photoexcitation system does not require simultaneous satisfactory for both proton reduction and water oxidation reactions. In a Z-scheme water-splitting system, an electronic mediator is used to drive the redox cycle between H_2-evolution photocatalyst and O_2-evolution photocatalyst. This is quite different from the single-step excitation photocatalyst for overall water splitting, in which the band structure of the photocatalyst must at least straddle the chemical potentials for proton reduction and water oxidation thermodynamically.

The two-step excitation water-splitting (Z-scheme) system composed of hydrogen-evolution photocatalyst (HEP), oxygen-evolution photocatalyst (OEP), and electronic mediator was first reported by Sayama and coworkers *(119)*. Under visible light irradiation, they found that the H_2 evolution took place on a metal-doped $SrTiO_3$ photocatalyst, while Pt–WO_3 photocatalyst shows an excellent activity in O_2 evolution. The I^-/IO_3^- redox couple was used as charge mediator. In this system, H_2 and O_2 evolved in the stoichiometric ratio ($H_2/O_2 = 2$) for more than 250 h, and the AQE was reported to be ca. 0.1% at 420 nm. Since then, more and more efficient Z-scheme systems for overall water splitting have been reported, as reviewed by Meada years ago *(120)*. For example, Pt-loaded ZrO_2/TaON and WO_3 photocatalysts are used as H_2 evolution and O_2 evolution photocatalysts, respectively, and I^-/IO_3^- acts as redox mediator for Z-scheme overall water-splitting system, which exhibits an AQE of 6.3% at 420 nm (Fig. 26) *(121)*.

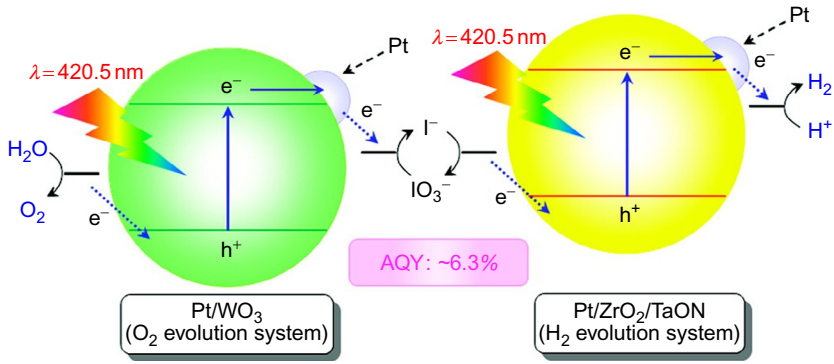

Fig. 26 Scheme of Z-scheme water-splitting system. *Reprinted (adapted) with permission from Maeda, K.; Higashi, M.; Lu, D. L.; Abe, R.; Domen, K.* J. Am. Chem. Soc., ***2010***, 132, *5858–5868. Copyright (2010) American Chemical Society.*

Recently, Chen et al. reported a Z-scheme water splitting system using $MgTa_2O_{6-x}N_y$/TaON heterojunction photocatalyst as H_2-evolution photocatalyst and achieved an AQE as high as 6.8% at 420 nm, which is the highest AQE for Z-scheme water splitting reported so far *(122)*.

In the Z-scheme water-splitting systems, another confusing issue is that the reverse reaction between photogenerated charges and soluble redox mediators suppressing the desired gas evolution. Reduction of electronic mediators competes with proton reduction reaction, and the oxidation of electronic mediators competes with O_2 evolution reaction. Such competition reactions suppress the charge utilization efficiency for overall water splitting. Taking the Fe^{3+}/Fe^{2+} mediator as an example, the reverse reactions in Z-scheme water-splitting systems include following reactions:

$$2H_2 + O_2 \rightarrow 2H_2O$$
$$H_2 + 2Fe^{3+} \rightarrow 2H^+ + 2Fe^{2+}$$
$$O_2 + 4Fe^{2+} + 4H^+ \rightarrow 2H_2O + 4Fe^{3+}$$

The produced H_2 and O_2 in Z-scheme water-splitting system can not only form H_2O molecule but also react with Fe^{2+} or Fe^{3+} shuttle ions in the solution. Depositing proper cocatalyst on the surface of photocatalyst is one of the useful strategies to inhibit the reverse reaction. For a Z-scheme photocatalyst using $SrTiO_3$:Rh and $BiVO_4$ for hydrogen and oxygen evolution, and Fe^{2+}/Fe^{3+} as electronic mediator, the effect of cocatalyst on reverse reaction was discussed (Fig. 27) *(123)*. The performance of overall water splitting was gradually decreased as the reaction proceeds when Pt cocatalyst was deposited on the surface of $SrTiO_3$:Rh photocatalyst, which is due to H_2O formation from the produced H_2 and O_2 as demonstrated by the significant decreases in H_2 and O_2 pressures. When Ru cocatalyst was deposited in place of Pt, the reverse reaction is inhibited almost completely, and the H_2 and O_2 evolution is maintained without obvious decrease. In control experiments, H_2 and O_2 are no longer consumed in the system after Ru cocatalyst loaded in the absence and presence of Fe^{3+} ions cases (Fig. 27C). It is a good example showing that the proper cocatalyst is important for optimizing both reduction and oxidation reactions, improving the stability and suppressing reverse reactions in Z-scheme water-splitting systems using soluble mediators.

In order to restrain the reverse reactions in Z-scheme water-splitting systems, proton reduction and water oxidation reactions can also be separated by introducing proton exchange membrane. For example, Fujihara and Matsumura et al. reported simultaneous H_2 and O_2 evolution using a

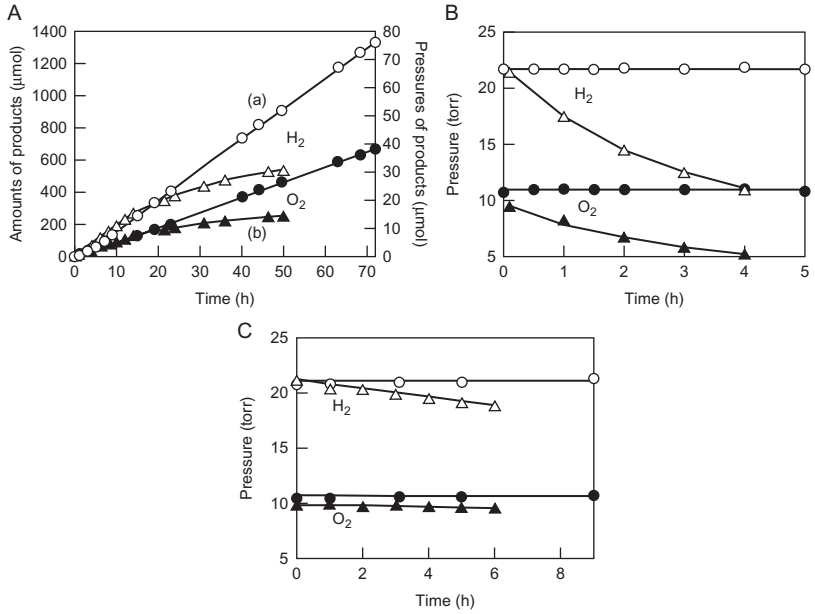

Fig. 27 Reverse reaction in Z-scheme water-splitting system. (A) Photocatalytic overall water splitting on Ru/$SrTiO_3$:Rh-$BiVO_4$ and Pt/$SrTiO_3$:Rh-$BiVO_4$ systems; (B) reverse reaction of H_2 and O_2 without the presence of Fe^{3+} ions; (C) reverse reaction of H_2 and O_2 in the presence of Fe^{3+} ions. *Reprinted (adapted) with permission from Sasaki, Y.; Iwase, A.; Kato, H.; Kudo, A.* J. Catal.*,* ***2008****,* 259*, 133–137. Copyright (2008) Elsevier.*

two-compartment Z-scheme photoelectrochemical water-splitting cell separated by Nafion membrane *(124)*. In this system, H_2 evolves on Pt/rutile TiO_2 suspended in the cathode compartment using bromide as an electron donor, and O_2 evolution takes place on rutile TiO_2 dispersed in the anode compartment in the presence of Fe^{3+} as an electron donor. Fe^{2+} ions are oxidized by bromine at the electrodes, and the produced protons are transported through Nafion membranes to maintain the electric neutrality and pH of the solutions in the two compartments. As a result, water is continuously split into hydrogen and oxygen under light irradiation.

Additionally, to avoid the drawback of the soluble redox mediators in Z-scheme water splitting system, solid-state Z-scheme systems coupling two photocatalysts with solid-state mediators (e.g., Au, Ag) have been also studied. Very recently, using Au as electronic mediator, Wang and Domen et al. fabricated a photocatalyst sheet composing hydrogen-evolution photocatalyst ($SrTiO_3$:La,Rh) and oxygen-evolution photocatalyst ($BiVO_4$:Mo) (Fig. 28) *(125)*. The photocatalyst sheet displays an extremely

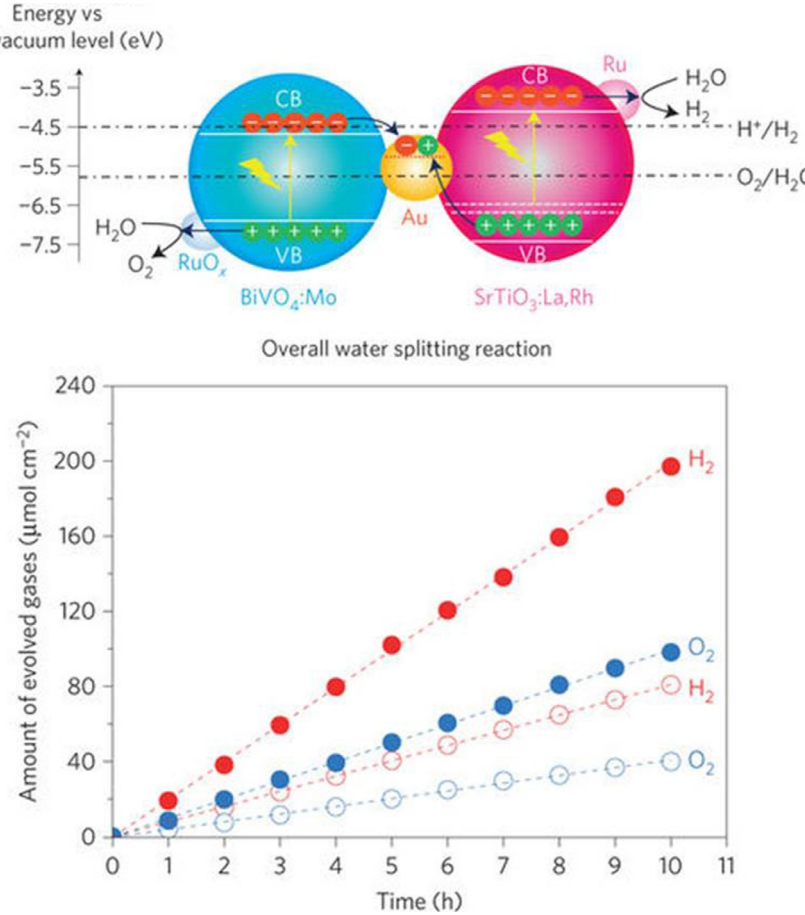

Fig. 28 Scheme of solid-state Z scheme overall water splitting using $SrTiO_3$:La,Rh as HEP, $BiVO_4$:Mo as OEP and Au as the electronic shuttle. *Reprinted (adapted) with permission from Wang, Q.; Hisatomi, T.; Jia, Q. X.; Tokudome, H.; Zhong, M.; Wang, C. Z.; Pan, Z. H.; Takata, T.; Nakabayashi, M.; Shibata, N.; Li, Y. B.; Sharp, I. D.; Kudo, A.; Yamada, T.; Domen, K.* Nat. Mater., ***2016***, 15, *611–615. Copyright (2016) Nature Publishing Group.*

high overall water-splitting activity with AQE of 30% at 419 nm and STH efficiency over 1%, which is the highest efficiency reported for particulate photocatalyst system. The challenge in developing a solid-state electronic mediator lies in achieving a dynamic equilibrium between the electron-accepting and -donating abilities of the mediator. Very recently, Wang et al. successfully constructed a solid-state Z scheme overall water splitting system using plasmoic photocatalyst Au-TiO_2 for O_2 evolution and

$SrTiO_3$:Rh for H_2 production. They found that Au nanoparticles on TiO_2 play bifunctional roles in this system, that is, not only act as visible light absorber induced by plasmon effect, but also function as efficient electron mediator for charge transfer *(126)*.

In comparison with the single photocatalyst system for photocatalytic water splitting, the advantages of the Z-scheme water-splitting system include: harvesting of a wider range of visible light using photocatalysts with narrower band gaps for H_2 or O_2 evolution, separation of H_2 and O_2 evolution on different semiconductor photocatalyst avoiding reverse reactions to a certain degree, and most importantly, much more flexibility in material screening since the proton reduction and water oxidation are separately considered on the two individual photocatalysts *(127)*. One may assemble an overall photocatalytic water-splitting system using photocatalysts which have sufficient energy only for water reduction or oxidation half reaction. For example, some metal oxides (e.g., WO_3, $BiVO_4$) are generally used as water oxidation photocatalysts, but they cannot reduce H^+ to H_2 due to their more positive conduction band positions than proton reduction, however, they can be used for constructing a Z-scheme overall water-splitting system.

8.3 Hybrid Natural–Artificial Photosynthesis System

Natural photosynthesis provides the blueprint for conversion and storage of solar energy in the form of chemical fuels (e.g., glucose, cellulose) *(128–131)*. Inspired by the nature system, assembling part of natural photosystem components with artificial photocatalyst to integrate a hybrid system has also been realized in recent years. A two-step photoexcitation natural–artificial hybrid photosystem was assembled, in which the PSII membrane fragments obtained from fresh spinach act as water oxidation catalyst, $SrTiO_3$:Rh as hydrogen production photocatalyst, and $Fe(CN)_6^{3-}/Fe(CN)_6^{4-}$ donor/acceptor pair acts as electronic mediator (Fig. 29) *(132)*. The hybrid system can achieve efficient overall water splitting (H_2/O_2 close to the stoichiometric ratio) under sunlight irradiation. It indicates that it is possible to achieve efficient charge transfer from a biophotosystem to an artificial photocatalyst via the interaction between the natural PSII membrane and the semiconductor-based photocatalyst. Furthermore, a hybrid photoanode by integrating cyanobacterial photosystem II (PSII) on Fe_2O_3 photoanode has also been constructed, and the efficient electron transfer from PSII to Fe_2O_3 results in a

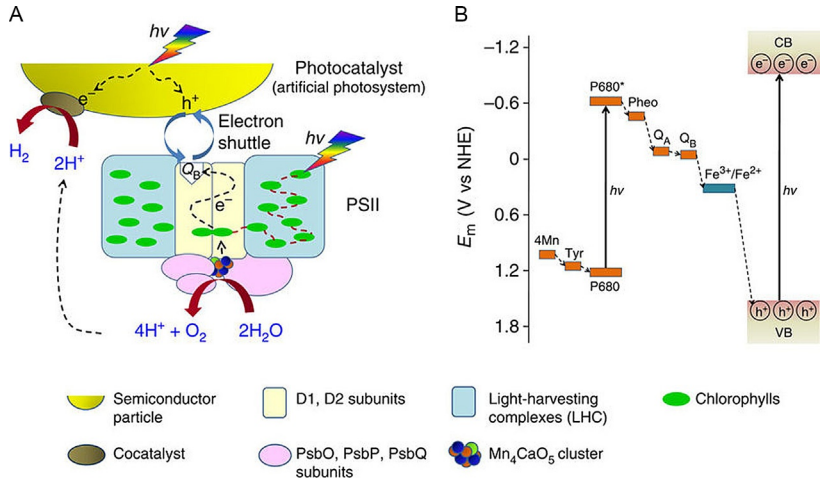

Fig. 29 Two-step photoexcitation natural–artificial hybrid photosystems integrated by PSII and artificial photocatalysts. *Reprinted (adapted) with permission from Wang, W. Y.; Chen, J.; Li, C.; Tian, W. M.* Nat. Commun. ***2014***, 5. *DOI:10.1038/ncomms5647. Copyright (2014) Nature Publishing Group.*

significant improvement in the performance of photoelectrochemical water splitting *(133)*.

9. TECHNICAL AND ECONOMIC EVALUATION FOR SOLAR WATER SPLITTING

Three kinds of commonly used solar water-splitting techniques, including particulate photocatalysis (PC) system, photoelectrocatalysis (PEC) system, and photovoltaic–electrochemical (PV–EC) hybrid system are schematically described in Fig. 30 *(134)*. For the PC system, the photocatalyst powders are needed to be dispersed in water pool for hydrogen production under the light irradiation, which is recognized as the simplest and low-cost one among all three systems. However, the highest STH efficiency for PC system at present is only ~1.0%. Moreover, the requirement of H_2/O_2 gas separation for safety issue and the enclosed reaction system are disadvantageous toward PC water splitting for potential large-scale application in the future. For PEC system, although the evolved H_2 and O_2 can be spatially separated on different electrodes by proton permeable membrane, the cost for the assembly of such PEC system is relatively higher than PC system. Fabrication of large area photoelectrodes and reactors will dramatically decrease the efficiency due to the possible introduction of more defects

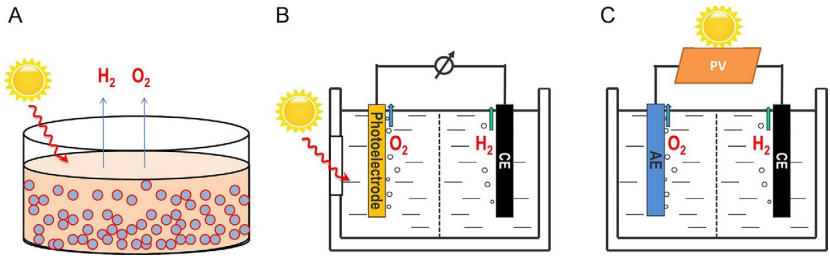

Fig. 30 Schematic description of solar water-splitting techniques for hydrogen production. (A) PC, (B) PEC, and (C) PV–EC systems. *Reprinted (adapted) with permission from Li, R. G.* Chin. J. Catal., ***2017***, 38, *5–12. Copyright (2017) Elsevier.*

in photoanode (cathode) materials. Moreover, an extra bias may be required to drive the overall PEC water-splitting reaction, which consequently increases the additional energy costs. Up to date, the highest STH efficiency for PEC water splitting system as reported is ~2.5% in several typical photoanode systems, e.g., $BiVO_4$ *(135)*, Ta_3N_5 *(136)*. Alternatively, PV–EC hybrid system is a kind of tandem structure integrating photovoltaic solar cells with water-splitting electrocatalysts. The STH efficiency for PV–EC water splitting system has already exceeded more than 10% in many integrated systems, and the highest efficiency is ~30% reported so far *(137,138)*. Nevertheless, similar to the drawbacks of PEC system, fabrication of such a complex PV–EC system for hydrogen production from water splitting is still not cost-competitive and easily operable. A qualitative comparison of operability, cost, and STH efficiency for three solar water-splitting techniques is briefly summarized in Table 1. Overall, none of the solar water-splitting technology developed in the laboratory scale can be competitive enough to be commercialized under the current economic situations. However, with the depletion of the fossil fuels, increasing price of the fossil fuels and the fast advances of the sciences and technology for solar water-splitting research field, it is quite feasible that the cost of hydrogen production via solar water splitting will be competitive with the hydrogen produced from traditional fossil fuels in the near future.

In 2011, the United States Department of Energy (US-DOE) reported that the maximum cost of hydrogen in 2020 that would make solar produced hydrogen as a viable fuel would be \$2–4 USD kg^{-1}. At present, the hydrogen cost target for 2020 generated by PEC systems is \$5.7 USD kg^{-1}, and further decreasing to \$2.1 USD kg^{-1} is anticipated in the more distant future. In 2008, the Ministry of Economy, Trade, and Industry (METI) of Japan suggested a similar value of 40 JPY Nm^{-3} as a hydrogen cost target

Table 1 Comparison of Solar Water-Splitting Techniques for Hydrogen Production

System	Cost	STH Efficiency	Examples	References
PC	Low	Low (<1.0%)	$SrTiO_3$:Rh/Au/ $BiVO_4$;$(Ga_{1-x}Zn_x)(N_{1-x}O_x)$	*(114,136)*
PEC	Medium	Medium (~2.5%)	FeOOH/NiOOH/$BiVO_4$ $Ni(OH)_x$/Fh/TiO_x/Ta_3N_5	*(133,135)*
PV–EC	High	High (>10%)	GaInP/GaAs/Ge-Ni electrode InGaP/GaAs/GaInNAsSb-PEM electrode	*(137, 138)*

in 2020. Researchers from universities and national labs of the United States promoted a technical and economic analysis of the cost of solar hydrogen production by various types of photocatalytic and PEC systems in 2013 *(121)*. Assuming an STH of 10% and a lifetime of 10 years for these systems, the price of hydrogen was estimated to be 1.6–10.4 USD kg^{-1}. Particulate photocatalyst systems with simple plastic bag reactors are expected to be less expensive than PEC systems and could potentially meet the DOE target hydrogen price of 2–4 USD kg^{-1}. The price of hydrogen production via PV–EC is the most expensive one, but leveraging the knowledge from the PV industry increases the cost certainty for components such as panel fabrication and encapsulation costs, it is roughly estimated to be 4–10 USD kg^{-1}. It is still very challenging to achieve both a high STH and the safe separation of hydrogen and oxygen with these devices. For PEC and PV–EC systems, they can achieve high STH values but have the associated challenge of high capital costs. Further improvement in STH efficiency as well as reductions in the costs of fabricating these solar water splitting devices is therefore required in addition to demonstrations of long-term stability.

10. CONCLUSION AND OUTLOOK

Up to now, extensive efforts have been made, and significant advances have been achieved in the research on photocatalytic water splitting, including exploration of suitable materials for light harvesting, strategies for photogenerated charge separation, and efficient cocatalysts for proton reduction and water oxidation reactions.

(1) In order to harvest more solar light by a photocatalyst, various approaches (e.g., band gap engineering) have been developed to extend

the light absorption range of photocatalyst from UV to visible even near IR region. It still remains challenging to achieve overall water splitting on photocatalyst capable of absorbing a wide range of visible light, e.g., the absorption range is larger than 600 nm. Exploring new materials and strategies to extend the absorption range of photocatalysts are still significant topics in the field of solar water splitting currently. Moreover, new methodology for designing and synthesizing visible light-responsive photocatalysts, systematic theoretical prediction of novel structured photocatalysts will also be instructive for the research of solar-to-chemical energy conversion.

(2) Photogenerated charge separation is a long-standing issue in photocatalysis. The present strategies for spatial charge separation, e.g., p–n junction, heterojunction, phase junction, and spatial charge separation between different facets have been widely used and well-recognized in photocatalysis. Novel strategies for efficient charge separation are still imperatively needed to be explored to aid the design and fabrication of highly efficient photocatalytic systems. Meanwhile, advanced ultrafast and in situ spectroscopies are strongly desired to probe the fast charge separation process in different timescales. It is also of vital importance to simulate the charge separation process and dynamics with the assistance of theoretical calculations.

(3) Efficient cocatalysts, especially water oxidation cocatalysts, deserve to be developed for constructing photocatalytic water-splitting systems. Dual-cocatalyst strategy has been demonstrated to be a general strategy in many photocatalyst systems in photocatalysis. Cocatalysts with controllable particle size from (quasi) single atom, clusters to nanometer scales will be essential for recognizing the actual roles of cocatalysts and how the catalytic reactions take place at the molecular level. Learning and mimicking from the structures of active sites in natural photosynthesis system for designing efficient artificial photocatalysts, especially water oxidation cocatalysts will be one of fascinating topics in artificial photosynthesis. The reverse reactions, that is, H_2 and O_2 for generating H_2O, and the interaction between photogenerated charges and mediators in Z-scheme systems are still big challenges in photocatalytic water splitting. A highly efficient photocatalyst system could be achieved by rationally depositing proper dual-cocatalysts, optimizing both reduction and oxidation reactions and suppressing the reverse reactions, etc. Investigating the kinetics of catalytic reactions will provide useful information for understanding the mechanism of photocatalytic water splitting.

There are still many challenging scientific issues that urgently required to be addressed in the research of photocatalyic water splitting, e.g., how the photogenerated charge separation takes place in the bulk of photocatalyst at a very fast timescale, how is the H–O bond broken at the initial stage of reaction, how are H–H and O–O bonds formed on the surface of photocatalyst, and how to accurately simulate the charge separation process and catalytic reaction by theoretical calculation in photocatalysis. These fundamental researches will help us to deeply understand the mechanism and further provide guidance for constructing highly efficient solar energy conversion systems. It is strongly believed that the continuous and extensive research in this area will result in the development of highly efficient, robust, cheap, and scalable photocatalyst systems in the near future, thus achieving a carbon free and sustainable earth for human beings.

ACKNOWLEDGMENTS

The authors would like to thank Prof. Hongxian Han for his suggestions and language polishing. This work was financially supported by 973 National Basic Research Program of the Ministry of Science and Technology (2014CB239400), National Natural Science Foundation of China (21501236, 21633010, 21673230), Dalian Institute of Chemical Physics (DICP ZZBS201610), National Natural Science Foundation of Liaoning province (201602739), and Youth Innovation Promotion Association of Chinese Academy of Sciences (2016167).

REFERENCES

1. Walter, M. G.; Warren, E. L.; McKone, J. R.; Boettcher, S. W.; Mi, Q. X.; Santori, E. A.; Lewis, N. S. *Chem. Rev.* **2010**, *110*, 6446–6473.
2. Momirlan, M.; Veziroglu, T. N. *Int. J. Hydrogen Energy* **2005**, *30*, 795–802.
3. Bak, T.; Nowotny, J.; Rekas, M.; Sorrell, C. *Int. J. Hydrogen Energy* **2002**, *27*, 19–26.
4. Bak, T.; Nowotny, J.; Rekas, M.; Sorrell, C. *Int. J. Hydrogen Energy* **2002**, *27*, 991–1022.
5. Jessop, P. G.; Ikariya, T.; Noyori, R. *Chem. Rev.* **1995**, *95*, 259–272.
6. Ashley, A. E.; Thompson, A. L.; O'Hare, D. *Angew. Chem. Int. Ed.* **2009**, *48*, 9839–9843.
7. Dorner, R. W.; Hardy, D. R.; Williams, F. W.; Willauer, H. D. *Energ. Environ. Sci.* **2010**, *3*, 884–890.
8. Fujishima, A.; Honda, K. *Nature* **1972**, *238*, 37–38.
9. Linsebigler, A. L.; Lu, G.; Yates, J. T., Jr. *Chem. Rev.* **1995**, *95*, 735–758.
10. Chen, X.; Mao, S. S. *Chem. Rev.* **2007**, *107*, 2891–2959.
11. Chen, X.; Shen, S.; Guo, L.; Mao, S. S. *Chem. Rev.* **2010**, *110*, 6503–6570.
12. Hisatomi, T.; Kubota, J.; Domen, K. *Chem. Soc. Rev.* **2014**, *43*, 7520–7535.
13. Serpone, N. *J. Photochem. Photobiol. A Chem.* **1997**, *104*, 1–12.
14. Kudo, A.; Miseki, Y. *Chem. Soc. Rev.* **2009**, *38*, 253–278.
15. Sayama, K.; Arakawa, H. *J. Chem. Soc. Faraday Trans.* **1997**, *93*, 1647–1654.
16. Maeda, K. *Chem. Commun.* **2013**, *49*, 8404–8406.

17. Li, R. G.; Weng, Y. X.; Zhou, X.; Wang, X. L.; Mi, Y.; Chong, R. F.; Han, H. X.; Li, C. *Energ. Environ. Sci.* **2015**, *8*, 2377–2382.
18. Konta, R.; Ishii, T.; Kato, H.; Kudo, A. *J. Phys. Chem. B* **2004**, *108*, 8992–8995.
19. Kato, H.; Kudo, A. *J. Phys. Chem. B* **2002**, *106*, 5029–5034.
20. Mu, L. C.; Zhao, Y.; Li, A. L.; Wang, S. Y.; Wang, Z. L.; Yang, J. X.; Wang, Y.; Liu, T. F.; Chen, R. T.; Zhu, J.; Fan, F. T.; Li, R. G.; Li, C. *Energ. Environ. Sci.* **2016**, *9*, 2463–2469.
21. Ham, Y.; Hisatomi, T.; Goto, Y.; Moriya, Y.; Sakata, Y.; Yamakata, A.; Kubota, J.; Domen, K. *J. Mater. Chem. A* **2016**, *4*, 3027–3033.
22. Miseki, Y.; Kato, H.; Kudo, A. *Energ. Environ. Sci.* **2009**, *2*, 306–314.
23. Kato, H.; Kudo, A. *J. Phys. Chem. B* **2001**, *105*, 4285–4292.
24. Kato, H.; Asakura, K.; Kudo, A. *J. Am. Chem. Soc.* **2003**, *125*, 3082–3089.
25. Sayama, K.; Arakawa, H. *J. Photochem. Photobiol. A Chem.* **1994**, *77*, 243–247.
26. Kurihara, T.; Okutomi, H.; Miseki, Y.; Kato, H.; Kudo, A. *Chem. Lett.* **2006**, *35*, 274–275.
27. Kudo, A.; Kato, H. *Chem. Lett.* **1997**, *26*(9), 867–868.
28. Kato, H.; Kudo, A. *Chem. Lett.* **1999**, *28*(11), 1207–1208.
29. Kudo, A.; Tanaka, A.; Domen, K.; Maruya, K.; Aika, K.; Onishi, T. *J. Catal.* **1988**, *111*, 67–76.
30. Kudo, A.; Kato, H.; Nakagawa, S. *J. Phys. Chem. B* **2000**, *104*, 571–575.
31. Kudo, A.; Nakagawa, S.; Kato, H. *Chem. Lett.* **1999**, *28*(11), 1197–1198.
32. Miseki, Y.; Kato, H.; Kudo, A. *Chem. Lett.* **2006**, *35*, 1052–1053.
33. Abe, R.; Higashi, M.; Zou, Z. G.; Sayama, K.; Abe, Y.; Arakawa, H. *J. Phys. Chem. B* **2004**, *108*, 811–814.
34. Sayama, K.; Arakawa, H. *J. Phys. Chem.* **1993**, *97*, 531–533.
35. Sato, J.; Saito, N.; Nishiyama, H.; Inoue, Y. *J. Phys. Chem. B* **2001**, *105*, 6061–6063.
36. Asahi, R.; Morikawa, T.; Ohwaki, T.; Aoki, K.; Taga, Y. *Science* **2001**, *293*, 269–271.
37. Liu, G.; Zhao, Y.; Sun, C.; Li, F.; Lu, G. Q.; Cheng, H. M. *Angew. Chem. Int. Ed.* **2008**, *47*, 4516–4520.
38. Chen, S. S.; Qi, Y.; Liu, G. J.; Yang, J. X.; Zhang, F. X.; Li, C. *Chem. Commun.* **2014**, *50*, 14415–14417.
39. Chen, S. S.; Yang, J. X.; Ding, C. M.; Li, R. G.; Jin, S. Q.; Wang, D. E.; Han, H. X.; Zhang, F. X.; Li, C. *J. Mater. Chem. A* **2013**, *1*, 5651–5659.
40. Hitoki, G.; Takata, T.; Kondo, J. N.; Hara, M.; Kobayashi, H.; Domen, K. *Chem. Commun.* **2002**, 1698–1699.
41. Hitoki, G.; Ishikawa, A.; Takata, T.; Kondo, J. N.; Hara, M.; Domen, K. *Chem. Lett.* **2002**, *31*(7), 736–737.
42. Ishikawa, A.; Takata, T.; Kondo, J. N.; Hara, M.; Kobayashi, H.; Domen, K. *J. Am. Chem. Soc.* **2002**, *124*, 13547–13553.
43. Ishikawa, A.; Takata, T.; Matsumura, T.; Kondo, J. N.; Hara, M.; Kobayashi, H.; Domen, K. *J. Phys. Chem. B* **2004**, *108*, 2637–2642.
44. Suzuki, T.; Hisatomi, T.; Teramura, K.; Shimodaira, Y.; Kobayashi, H.; Domen, K. *Phys. Chem. Chem. Phys.* **2012**, *14*, 15475–15481.
45. Ouyang, S. X.; Kikugawa, N.; Chen, D.; Zou, Z. G.; Ye, J. H. *J. Phys. Chem. C* **2009**, *113*, 1560–1566.
46. Ouyang, S. X.; Ye, J. H. *J. Am. Chem. Soc.* **2011**, *133*, 7757–7763.
47. Maeda, K.; Takata, T.; Hara, M.; Saito, N.; Inoue, Y.; Kobayashi, H.; Domen, K. *J. Am. Chem. Soc.* **2005**, *127*, 8286–8287.
48. Hirai, T.; Maeda, K.; Yoshida, M.; Kubota, J.; Ikeda, S.; Matsumura, M.; Domen, K. *J. Phys. Chem. C* **2007**, *111*, 18853–18855.
49. Lee, Y.; Terashima, H.; Shimodaira, Y.; Teramura, K.; Hara, M.; Kobayashi, H.; Domen, K.; Yashima, M. *J. Phys. Chem. C* **2007**, *111*, 1042–1048.

50. Marschall, R. *Adv. Funct. Mater.* **2014**, *24*, 2421–2440.
51. Wang, H.; Zhang, L.; Chen, Z.; Hu, J.; Li, S.; Wang, Z.; Liu, J.; Wang, X. *Chem. Soc. Rev.* **2014**, *43*, 5234–5244.
52. Jang, J. S.; Kim, H. G.; Lee, J. S. *Catal. Today* **2012**, *185*, 270–277.
53. Nozik, A. J. *Appl. Phys. Lett.* **1976**, *29*, 150–153.
54. Chen, S. F.; Zhao, W.; Liu, W.; Zhang, S. J. *Appl. Surf. Sci.* **2008**, *255*, 2478–2484.
55. Kim, H. G.; Borse, P. H.; Choi, W. Y.; Lee, J. S. *Angew. Chem. Int. Ed.* **2005**, *44*, 4585–4589.
56. Kim, H. G.; Borse, P. H.; Jang, J. S.; Jeong, E. D.; Jung, O. S.; Suh, Y. J.; Lee, J. S. *Chem. Commun.* **2009**, 5889–5891.
57. Tristao, J. C.; Magalhaes, F.; Corio, P.; Sansiviero, M. T. C. *J. Photochem. Photobiol. A Chem.* **2006**, *181*, 152–157.
58. Srinivasan, S. S.; Wade, J.; Stefanakos, E. K. *J. Nanomater.* **2006**, *2006*(87326), 1–7.
59. Rao, P. M.; Cai, L. L.; Liu, C.; Cho, I. S.; Lee, C. H.; Weisse, J. M.; Yang, P. D.; Zheng, X. L. *Nano Lett.* **2014**, *14*, 1099–1105.
60. Su, J. Z.; Guo, L. J.; Bao, N. Z.; Grimes, C. A. *Nano Lett.* **2011**, *11*, 1928–1933.
61. Chatchai, P.; Murakami, Y.; Kishioka, S. Y.; Nosaka, A. Y.; Nosaka, Y. *Electrochim. Acta* **2009**, *54*, 1147–1152.
62. Gao, X. F.; Li, H. B.; Sun, W. T.; Chen, Q.; Tang, F. Q.; Peng, L. M. *J. Phys. Chem. C* **2009**, *113*, 7531–7535.
63. Seabold, J. A.; Shankar, K.; Wilke, R. H. T.; Paulose, M.; Varghese, O. K.; Grimes, C. A.; Choi, K. S. *Chem. Mater.* **2008**, *20*, 5266–5273.
64. Moniz, S. J. A.; Shevlin, S. A.; An, X. Q.; Guo, Z. X.; Tang, J. W. *Chem. A Eur. J.* **2014**, *20*, 15571–15579.
65. Peng, L. L.; Xie, T. F.; Lu, Y. C.; Fan, H. M.; Wang, D. J. *Phys. Chem. Chem. Phys.* **2010**, *12*, 8033–8041.
66. Sharma, D.; Upadhyay, S.; Satsangi, V. R.; Shrivastav, R.; Waghmare, U. V.; Dass, S. *J. Phys. Chem. C* **2014**, *118*, 25320–25329.
67. Wang, Y.; Yu, T.; Chen, X. Y.; Zhang, H. T.; Ouyang, S. X.; Li, Z. S.; Ye, J. H.; Zou, Z. G. *J. Phys. D Appl. Phys.* **2007**, *40*, 3925–3930.
68. Bai, S. L.; Zhang, K. W.; Sun, J. H.; Luo, R. X.; Li, D. Q.; Chen, A. F. *CrstEngComm* **2014**, *16*, 3289–3295.
69. Sivula, K.; Le Formal, F.; Gratzel, M. *Chem. Mater.* **2009**, *21*, 2862–2867.
70. Zhang, J.; Li, M.; Feng, Z.; Chen, J.; Li, C. *J. Phys. Chem. B* **2006**, *110*, 927–935.
71. Zhang, J.; Xu, Q.; Feng, Z.; Li, M.; Li, C. *Angew. Chem. Int. Ed.* **2008**, *47*, 1766–1769.
72. Ma, Y.; Xu, Q.; Zong, X.; Wang, D. G.; Wu, G. P.; Wang, X.; Li, C. *Energy Environ. Sci.* **2012**, *5*, 6345–6351.
73. Li, A. L.; Wang, Z. L.; Yin, H.; Wang, S. Y.; Yan, P. L.; Huang, B. K.; Wang, X. L.; Li, R. G.; Zong, X.; Han, H. X.; Li, C. *Chem. Sci.* **2016**, 7, 6076–6082.
74. Wang, X.; Xu, Q.; Li, M. R.; Shen, S.; Wang, X. L.; Wang, Y. C.; Feng, Z. C.; Shi, J. Y.; Han, H. X.; Li, C. *Angew. Chem. Int. Ed.* **2012**, *51*, 13089–13092.
75. Hou, J. G.; Yang, C.; Wang, Z.; Zhou, W. L.; Jiao, S. Q.; Zhu, H. M. *Appl. Catal. B Environ.* **2013**, *142*, 504–511.
76. Zhu, Y. Y.; Liu, Y. F.; Lv, Y. H.; Ling, Q.; Liu, D.; Zhu, Y. F. *J. Mater. Chem. A* **2014**, *2*, 13041–13048.
77. Lv, C. D.; Chen, G.; Sun, J. X.; Zhou, Y. S. *Inorg. Chem.* **2016**, *55*, 4782–4789.
78. Li, R. G.; Zhang, F. X.; Wang, D. G.; Yang, J. X.; Li, M. R.; Zhu, J.; Zhou, X.; Han, H. X.; Li, C. *Nat. Commun.* **2013**, *4*(1432), 1–7. https://doi.org/10.1038/ncomms2401.
79. Zhu, J.; Fan, F. T.; Chen, R. T.; An, H. Y.; Feng, Z. C.; Li, C. *Angew. Chem. Int. Ed.* **2015**, *54*, 9111–9114.

80. Pan, J.; Liu, G.; Lu, G. Q. M.; Cheng, H. M. *Angew. Chem. Int. Ed.* **2011**, *50*, 2133–2137.
81. Zheng, Z.; Huang, B.; Lu, J.; Qin, X.; Zhang, X.; Dai, Y. *Chem. A Eur. J.* **2011**, *17*, 15032–15038.
82. Yu, J.; Low, J.; Xiao, W.; Zhou, P.; Jaroniec, M. *J. Am. Chem. Soc.* **2014**, *136*, 8839–8842.
83. Li, N. X.; Liu, M. C.; Zhou, Z. H.; Zhou, J. C.; Sun, Y. M.; Guo, L. J. *Nanoscale* **2014**, *6*, 9695–9702.
84. Zhen, C.; Yu, J. C.; Liu, G.; Cheng, H. M. *Chem. Commun.* **2014**, *50*, 10416–10419.
85. Liu, G.; Yu, J. C.; Lu, G. Q.; Cheng, H. M. *Chem. Commun.* **2011**, *47*(24), 6763–6783.
86. Zhang, Q.; Li, R. G.; Li, Z.; Li, A. L.; Wang, S. Y.; Liang, Z. X.; Liao, S. J.; Li, C. *J. Catal.* **2016**, *337*, 36–44.
87. Zhang, L.; Wang, W. Z.; Sun, S. M.; Jiang, D.; Gao, E. P. *Appl. Catal. B Environ.* **2015**, *162*, 470–474.
88. Ma, G. J.; Liu, J. Y.; Hisatomi, T.; Minegishi, T.; Moriya, Y.; Iwase, M.; Nishiyama, H.; Katayama, M.; Yamada, T.; Domen, K. *Chem. Commun.* **2015**, *51*, 4302–4305.
89. Ma, Y.; Wang, X. L.; Jia, Y. S.; Chen, X. B.; Han, H. X.; Li, C. *Chem. Rev.* **2014**, *114*, 9987–10043.
90. Zhang, F. X.; Yamakata, A.; Maeda, K.; Moriya, Y.; Takata, T.; Kubota, J.; Teshima, K.; Oishi, S.; Domen, K. *J. Am. Chem. Soc.* **2012**, *134*, 8348–8351.
91. Singh, R. B.; Matsuzaki, H.; Suzuki, Y.; Seki, K.; Minegishi, T.; Hisatomi, T.; Domen, K.; Furube, A. *J. Am. Chem. Soc.* **2014**, *136*, 17324–17331.
92. Yamakata, A.; Kawaguchi, M.; Murachi, R.; Okawa, M.; Kamiya, I. *J. Phys. Chem. C* **2016**, *120*, 7997–8004.
93. Grigioni, I.; Stamplecoskie, K. G.; Selli, E.; Kamat, P. V. *J. Phys. Chem. C* **2015**, *119*, 20792–20800.
94. Yang, J. H.; Wang, D. G.; Han, H. X.; Li, C. *Acc. Chem. Res.* **2013**, *46*, 1900–1909.
95. Yan, H. J.; Yang, J. H.; Ma, G. J.; Wu, G. P.; Zong, X.; Lei, Z. B.; Shi, J. Y.; Li, C. *J. Catal.* **2009**, *266*, 165–168.
96. Maeda, K.; Xiong, A. K.; Yoshinaga, T.; Ikeda, T.; Sakamoto, N.; Hisatomi, T.; Takashima, M.; Lu, D. L.; Kanehara, M.; Setoyama, T.; Teranishi, T.; Domen, K. *Angew. Chem. Int. Ed.* **2010**, *49*, 4096–4099.
97. Ma, B. J.; Wen, F. Y.; Jiang, H. F.; Yang, J. H.; Ying, P. L.; Li, C. *Catal. Lett.* **2010**, *134*, 78–86.
98. Lin, F.; Wang, D. G.; Jiang, Z. X.; Ma, Y.; Li, J.; Li, R. G.; Li, C. *Energy Environ. Sci.* **2012**, *5*, 6400–6406.
99. Li, R. G.; Han, H. X.; Zhang, F. X.; Wang, D. G.; Li, C. *Energy Environ. Sci.* **2014**, 7, 1369–1376.
100. Li, R. G.; Zhao, Y.; Li, C. *Faraday Discuss.* **2017**, *198*, 463–472.
101. Wang, D. E.; Li, R. G.; Zhu, J.; Shi, J. Y.; Han, J. F.; Zong, X.; Li, C. *J. Phys. Chem. C* **2012**, *116*, 5082–5089.
102. Maeda, K.; Teramura, K.; Lu, D. L.; Takata, T.; Saito, N.; Inoue, Y.; Domen, K. *Nature* **2006**, *440*, 295.
103. Maeda, K.; Teramura, K.; Lu, D. L.; Saito, N.; Inoue, Y.; Domen, K. *Angew. Chem. Int. Ed.* **2006**, *45*, 7806–7809.
104. Maeda, K.; Teramura, K.; Lu, D. L.; Takata, T.; Saito, N.; Inoue, Y.; Domen, K. *J. Phys. Chem. C* **2006**, *110*, 13753–13758.
105. Yoshida, M.; Takanabe, K.; Maeda, K.; Ishikawa, A.; Kubota, J.; Sakata, Y.; Ikezawa, Y.; Domen, K. *J. Phys. Chem. C* **2009**, *113*, 10151–10157.
106. Townsend, T. K.; Browning, N. D.; Osterloh, F. E. *Energy Environ. Sci.* **2012**, *5*, 9543–9550.

107. Zhang, Q.; Li, Z.; Wang, S.; Li, R.; Zhang, X.; Liang, Z.; Han, H.; Liao, S.; Li, C. *ACS Catal.* **2016**, *6*, 2182–2191.
108. Ma, Y.; Chong, R.; Zhang, F.; Xu, Q.; Shen, S.; Han, H.; Li, C. *Phys. Chem. Chem. Phys.* **2014**, *16*, 17734–17742.
109. Tang, J.; Durrant, J. R.; Klug, D. R. *J. Am. Chem. Soc.* **2008**, *130*, 13885–13891.
110. Nakamura, R.; Nakato, Y. *J. Am. Chem. Soc.* **2004**, *126*, 1290–1298.
111. Valde's, A.; Qu, Z.-W.; Kroes, G.-J.; Rossmeisl, J.; Nørskov, J. K. *J. Phys. Chem. C* **2008**, *112*, 9872–9879.
112. Sakata, Y.; Hayashi, T.; Yasunaga, R.; Yanaga, N.; Imamura, H. *Chem. Commun.* **2015**, *51*, 12935–12938.
113. Ham, Y.; Hisatomi, T.; Goto, Y.; Moriya, Y.; Sakata, Y.; Yamakata, A.; Kubota, J.; Domen, K. *J. Mater. Chem. A* **2016**, *4*, 3.027–3033.
114. Maeda, K.; Teramura, K.; Domen, K. *J. Catal.* **2008**, *254*, 198–204.
115. Zou, Z.; Ye, J.; Sayama, K.; Arakawa, H. *Nature* **2001**, *414*, 625–627.
116. Pan, C.; Takata, T.; Nakabayashi, M.; Matsumoto, T.; Shibata, N.; Ikuhara, Y.; Domen, K. A. *Angew. Chem. Int. Ed.* **2015**, *54*, 2955–2959.
117. Yeh, T. F.; Teng, C. Y.; Chen, S. J.; Teng, H. *Adv. Mater.* **2014**, *26*, 3297–3303.
118. Kibria, M. G.; Nguyen, H. P.; Cui, K.; Zhao, S.; Liu, D.; Guo, H.; Trudeau, M. L.; Paradis, S.; Hakima, A.-R.; Mi, Z. *ACS Nano* **2013**, 7, 7886–7893.
119. Sayama, K.; Mukasa, K.; Abe, R.; Abe, Y.; Arakawa, H. *J. Photochem. Photobiol. A Chem.* **2002**, *148*, 71–77.
120. Maeda, K. *ACS Catal.* **2013**, *3*, 1486–1503.
121. Maeda, K.; Higashi, M.; Lu, D. L.; Abe, R.; Domen, K. *J. Am. Chem. Soc.* **2010**, *132*, 5858–5868.
122. Chen, S. S.; Qi, Y.; Hisatomi, T.; Ding, Q.; Asai, T.; Li, Z.; Ma, S. S. K.; Zhang, F. X.; Domen, K.; Li, C. *Angew. Chem. Int. Ed.* **2015**, *54*, 8498–8501.
123. Sasaki, Y.; Iwase, A.; Kato, H.; Kudo, A. *J. Catal.* **2008**, *259*, 133–137.
124. Fujihara, K.; Ohno, T.; Matsumura, M. *J. Chem. Soc. Faraday Trans.* **1998**, *94*, 3705–3709.
125. Wang, Q.; Hisatomi, T.; Jia, Q. X.; Tokudome, H.; Zhong, M.; Wang, C. Z.; Pan, Z. H.; Takata, T.; Nakabayashi, M.; Shibata, N.; Li, Y. B.; Sharp, I. D.; Kudo, A.; Yamada, T.; Domen, K. *Nat. Mater.* **2016**, *15*, 611–615.
126. Wang, S. Y.; Gao, Y. Y.; Yu, Q.; Li, A. L.; Fan, F. T.; Li, C. *J. Catal.* **2017**, *354*, 250–257.
127. Maeda, K.; Domen, K. *J. Phys. Chem. Lett.* **2010**, *1*, 2655–2661.
128. Zhang, C. X.; Chen, C. H.; Dong, H. X.; Shen, J. R.; Dau, H.; Zhao, J. Q. A. *Science* **2015**, *348*, 690–693.
129. Long, S.; Humphries, S.; Falkowski, P. G. *Annu. Rev. Plant Biol.* **1994**, *45*, 633–662.
130. Haehnel, W. *Annu. Rev. Plant Physiol.* **1984**, *35*, 659–693.
131. Gust, D.; Moore, T. A.; Moore, A. L. *Acc. Chem. Res.* **2001**, *34*, 40–48.
132. Wang, W. Y.; Chen, J.; Li, C.; Tian, W. M. *Nat. Commun.* **2014**, *5*(5647), 1–8. https://doi.org/10.1038/ncomms5647.
133. Liu, G.; Ye, S.; Yan, P.; Xiong, F. Q.; Fu, P.; Wang, Z.; Chen, Z.; Shi, J.; Li, C. *Energy Environ. Sci.* **2016**, *9*, 1327–1334.
134. Li, R. G. *Chin. J. Catal.* **2017**, *38*, 5–12.
135. Kim, T. W.; Choi, K. S. *Science* **2014**, *343*, 990–994.
136. Bonke, S. A.; Wiechen, M.; MacFarlane, D. R.; Spiccia, L. *Energy Environ. Sci.* **2015**, *8*, 2791–2796.
137. Jia, J.; Seitz, L. C.; Benck, J. D.; Huo, Y.; Chen, Y.; Ng, J. W. D.; Bilir, T.; Harris, J. S.; Jaramillo, T. F. *Nat. Commun.* **2016, 1–6**, 7(13237), 1–6. https://doi.org/10.1038/ncomms13237.
138. Bonke, S. A.; Wiechen, M.; MacFarlane, D. R.; Spiccia, L. *Energy Environ. Sci.* **2015**, *8*, 2791–2796.

ABOUT THE AUTHORS

Can Li received his Ph.D. degree in Physical Chemistry from Dalian Institute of Chemical Physics, Chinese Academy of Sciences, in 1989, and he joined the same institute and was promoted to full professor in 1993. He did postdoctoral research at Northwestern University, USA and was visiting professor at Lehigh University, the University of Liverpool, and The Queensland University, and he was awarded the JSPS Professor at Waseda University, Tokyo University of Technology, and Hokkaido University. He was an invited professor at Université Pierre et Marie Curie, Paris VI. He was elected as a member of the Chinese Academy of Sciences in 2003, a member of the Academy of Science for Developing Countries (TWAS) in 2005, a foreign member of Academia European in 2008, and a Fellow of the Royal Society of Chemistry in 2008. He was the President of the International Association of Catalysis Societies (2008–2012) and the president of the Asia-Pacific Association of Catalysis Societies (2013–2016). Currently, he is the director of the Dalian National Laboratory for Clean Energy (DNL). Among the prestigious awards and honors recognizing his research include International Catalysis Award, the National Natural Science Prize, National Catalysis Award, the Ho Leung Ho Lee Prize (Hong Kong), National Petrochemical Prize and National Outstanding Scientist Award.

His research interests span spectroscopic characterization of catalysts (e.g., UV Raman, FT-IR, time-resolved spectroscopy) and catalytic reactions, environmental catalysis, heterogeneous chiral catalysis. Over the last two decade, his research has focused on photocatalytic and photoelectrocatalytic water splitting and CO_2 reduction. He has been the Editor-in-Chief of *Chinese Journal of Catalysis* since 2014, and an associate editor of *Chemical Communications*.

Rengui Li received his B.S. degree from Xiamen University in 2009, and Ph.D. degree from Dalian Institute of Chemical Physics, Chinese Academy of Sciences in 2014 under the supervision of Prof. Can Li. Then he joined the same institute and has been working as an associate professor at State Key Laboratory of Catalysis since 2014. He was honored with the Young Scientist Prize at International Congress on Catalysis in 2016. His research interest is mainly focused on the photocatalytic solar energy conversion. He has published more than 20 scientific papers in *Nature Commun.*, *Energy Environ. Sci.*, *Adv. Energy Mater.,* etc., with more than 1200 citations.